

1 **Accelerated Estimation ~~An Improved Parameterization~~**
2 **of Sea Spray-Mediated Heat Flux Using Gaussian**
3 **Quadrature: Case Studies with a Coupled CFSv2.0-WW3**
4 **System**

5 Ruizi Shi¹ and Fanghua Xu^{1*}

6 ¹ Department of Earth System Science, Ministry of Education Key Laboratory for Earth System
7 Modeling, Institute for Global Change Studies, Tsinghua University, Beijing, 100084, China.

8 **Correspondence to:* Fanghua Xu (fxu@mail.tsinghua.edu.cn)

9

10 **Abstract.** Sea spray-mediated heat flux plays an important role in air-sea heat transfer. Heat flux
11 integrated over droplet size spectrum can well simulate total heat flux induced by sea spray droplets.
12 Previously, a fast ~~algorithm of~~ spray-flux ~~scheme~~-assuming single-radius droplets (A15) was widely used
13 since the full-size spectrum integral is ~~computationally~~ ~~computational~~-expensive. Based on the Gaussian
14 Quadrature (GQ) method, a new fast ~~algorithm scheme~~-(SPRAY-GQ) of sea spray-mediated heat flux is
15 derived. The performance of SPRAY-GQ is evaluated by comparing heat fluxes with those estimated
16 from the widely-used A15. The new ~~algorithm scheme~~-shows a better agreement with the original
17 spectrum integral. To further evaluate the ~~numerical errors performance~~-of A15 and SPRAY-GQ, the
18 two ~~algorithms schemes~~-are implemented into a coupled CFSv2.0-WW3 system, and a series of 56-day
19 simulations in summer and winter are conducted and compared. The comparisons with satellite
20 measurements and reanalysis data show that the SPRAY-GQ ~~algorithm scheme~~ could ~~simulate-lead to~~
21 ~~air-sea heat flux~~-more reasonable ~~simulationy~~ than the A15 ~~algorithm scheme~~-~~by modifying air-sea heat~~
22 ~~flux~~. For experiments based on SPRAY-GQ, the sea surface temperature at mid-high latitudes of both
23 hemispheres, particularly in summer, is significantly improved compared with the experiments based on
24 A15. The simulation of 10-m wind speed and significant wave height at mid-low latitudes of the Northern
25 Hemisphere ~~after the first two weeks~~ is improved as well. The computational time of SPRAY-GQ is
26 about the same as that of A15. Thereby, the newly-developed SPRAY-GQ ~~algorithm scheme~~-has a
27 potential to be used for ~~improving air-sea~~~~calculation of~~~~calculate~~ ~~spray-mediated~~ heat flux in coupled
28 models.
29

30 **1 Introduction**

31 Sea spray droplets, ejected from oceans, include film drops, jet drops and spume drops (Veron, 2015).
32 The first two types of droplets are generated from bubble bursting caused by ocean surface wave breaking,
33 with radius ranging from 0.5 μm to 50 μm (Resch and Afeti, 1991; Thorpe, 1992; Melville, 1996; Spiel,
34 1997; Andreas, 1998; Lhuissier and Villermaux, 2012). Spume drops are generated by strong winds ($>$
35 7-11 m/s) which directly tear the wave crests, with larger radius ranging from tens to ~~hundreds~~
36 of micrometers ~~μm~~ (Koga, 1981; Andreas et al., 1995; Andreas, 1998). Sea spray droplets play an
37 important role in weather and climate processes (Fox-Kemper et al., 2022). On one hand, sea spray
38 droplets contribute to local marine aerosols and subsequently modify the local radiation balance (Fairall
39 et al., 1983; Burk, 1984; Fairall and Larsen, 1984). On the other hand, sea spray droplets affect the fluxes
40 of heat, momentum, salt, and freshwater between atmosphere and ocean (Andreas, 1992; Andreas et al.,
41 2008; Andreas, 2010; Andreas et al., 2015; Ling and Kao, 1976; Fairall et al., 1994; Andreas and
42 Decosmo, 2002).

43 The sea spray-mediated heat transfer mainly occurs within the droplet evaporation layer (DEL) near
44 the sea surface (Andreas and Decosmo, 1999, 2002; Fairall et al., 1994). Sea spray droplets with the same
45 temperature as ocean surface can lead to sensible heat flux in DEL, while water evaporated from these
46 droplets can further release latent heat to the atmosphere (Andreas, 1992; Borisenkov, 1974; Bortkovskii,
47 1973; Wu, 1974; Monahan and Van Patten, 1988; Ling and Kao, 1976). Part of the sea spray-mediated
48 sensible heat is absorbed by droplet evaporation, which further increases the air-sea temperature
49 difference, and thus increases the sea spray-mediated sensible heat flux (Fairall et al., 1994; Andreas and
50 Decosmo, 2002). Since strong winds produce more sea spray droplets with larger radius, sea spray-
51 mediated heat fluxes increase with wind speed (Fairall et al., 1994), and contribute more than 10% of the
52 total surface heat flux after reaching the threshold speed ($>$ 11 m/s for sensible heat flux and $>$ 13 m/s
53 for latent heat flux)(Andreas et al., 2008). In addition, when a droplet is released into the air, it is
54 accelerated due to surface winds (Edson and Andreas, 1997; Fairall et al., 1994; Van Eijk et al., 2011;
55 Wu et al., 2017). If the droplet could fall back into the ocean, additional momentum would be injected
56 into the ocean from the atmosphere (Andreas, 1992, 2004).

57 The usual bulk parameterizations in numerical models for surface fluxes only include the interfacial

58 (turbulent) fluxes (e.g., Fairall et al., 1996), while neglecting the significant contributions of sea spray
59 droplets in DEL (Andreas et al., 2008; Fairall et al., 1994; Smith, 1997; Emanuel, 1995). Andreas and
60 Emanuel (2001) implemented sea spray-mediated heat flux and momentum flux parameterizations into
61 a simple tropical cyclone model, ~~and found that the sea spray-induced heat flux significantly enhances~~
62 ~~the tropical cyclone intensity, offsetting the negative effect of enhanced surface drag by strong wind and~~
63 ~~waves. They, and found that the sea spray-mediated induced heat flux can significantly enhance tropical~~
64 ~~cyclone intensity. It is well known that The strong winds and high waves induced by tropical cyclones~~
65 ~~can enhance sea surface roughness and thus surface drag coefficients, which tend to reduce tropical~~
66 ~~cyclone intensity (Emanuel, 1995). In addition~~ Furthermore, the accelerated sea spray droplets by
67 ~~surface winds also lead to more dissipation of tropical cyclone kinetic energy (Andreas, 1992, 2004).~~
68 ~~Andreas and Emanuel (2001) found that the sea spray-induced heat flux significantly enhances the~~
69 ~~tropical cyclone intensity, offsetting~~ These negative effects could be offset by the sea spray-
70 ~~mediated induced heat flux.~~ The similar enhancement of tropical cyclone intensity was also ~~shown~~
71 ~~noticed~~ in recent regional coupling systems by including sea spray-mediated heat flux (Xu et al., 2021b;
72 Liu et al., 2012; Garg et al., 2018; Zhao et al., 2017). In the First Institute of Oceanography Earth System
73 Model, Bao et al. (2020) first incorporated the sea spray-mediated heat flux in global climate simulation.
74 Following Bao et al. (2020), Song et al. (2022) found that the sea spray-mediated heat flux can lead to
75 cooling at the air-sea interface and strengthening westerlies in the Southern Ocean, and thus improves
76 estimates of sea surface temperature (SST).

77 Since the parameterization of sea spray-mediated heat flux derived from observations requires full-
78 size spectral integral and ~~thus is too computationally expensive-intensive for large-scale~~
79 ~~modelsdemands huge amount of computational time~~ (Table 1, details in Section 4.2; Andreas, 1989,
80 1990, 1992; Andreas et al., 2015), a simplified ~~algorithm parameterization~~ based on a single radius of
81 sea spray droplets (Andreas et al., 2015; Andreas et al., 2008) is widely used in atmosphere-ocean
82 coupling systems (Xu et al., 2021b; Liu et al., 2012; Garg et al., 2018; Zhao et al., 2017; Song et al.,
83 2022; Bao et al., 2020), and apt to produce ~~numerical errors~~ significant biases. To reduce ~~these numerical~~
84 ~~errors biases~~ induced by the single radius of sea spray droplets, we develop a new fast algorithm
85 parameterization of sea spray-mediated heat flux based on the Gaussian Quadrature (GQ) method, a fast

86 and accurate way to calculate spectral integral. The GQ method has been successfully used for the
87 estimation of domain-averaged radiative flux profiles (Li and Barker, 2018). The performance of the
88 GQ-based ~~fast algorithm parameterization~~ of the sea spray-mediated heat flux is evaluated and compared
89 with the simplified ~~algorithm parameterization~~ for single radius of Andreas et al. (2015), referred to as
90 A15 hereafter. The results are first compared with the original parameterization using full-size spectral
91 integral (A92, hereafter). Then the parameterizations ~~with different algorithms~~ are implemented in a
92 global coupled atmosphere-ocean-wave system (Shi et al., 2022), and the results are compared with
93 global satellite measurements and reanalysis data.

94 The rest of the paper is structured as follows: observation and reanalysis data for comparisons are
95 introduced in Section 2; the derivation of the GQ-based ~~fast algorithm parameterization~~ and the global
96 coupling system are described in Section 3; the performance of the new ~~fast algorithm parameterization~~
97 is evaluated in Section 4. Finally, a summary and discussion are given in Section 5.

98 **2 Data**

99 The fifth generation European Centre for Medium-Range Weather Forecasts (ECMWF) Reanalysis
100 (ERA5; Hersbach et al., 2020) ~~data assimilated huge amounts of historical data and thus provided reliable~~
101 ~~hourly estimates.~~ ERA5 10-m wind speed (WSP10), 2-m air temperature (~~T02~~), 2-m dewpoint
102 temperature, surface pressure and significant wave height (SWH) with a spatial resolution of 0.5° are
103 used. Additionally, WSP10, ~~T02-m air temperature~~ and 2-m specific humidity (~~SPH~~) data from the
104 Objectively Analyzed air-sea Fluxes (OAFflux) products (Yu et al., 2008) are also applied for comparison,
105 with 1°×1° resolution. The daily average satellite Optimum Interpolation SST (OISST) data are obtained
106 from the National Oceanic and Atmospheric Administration (NOAA) with a spatial resolution of 0.25°
107 (Reynolds et al., 2007). The global monthly mean salinity observations ~~s~~ from European Space Agency
108 (ESA; https://climate.esa.int/sites/default/files/SSS_cci-D1.1-URD-v1r4_signed-accepted.pdf) are
109 applied. ~~Besides, we also use the monthly global ocean RSS Satellite Data Products for WSP10~~
110 ~~(https://data.remss.com/wind/monthly_1deg/)—for—WSP10 and the Reprocessed L4 Satellite~~
111 ~~Measurements for SWH (<https://doi.org/10.48670/moi-00177>), to validate the our simulation results and~~
112 ~~ERA5 data.~~

113 3 Methods

114 3.1 Development of a Fast Algorithm Based on GQ

115 The effects of sea spray droplets on sensible and latent heat fluxes ($H_{S,SP}$, $H_{L,SP}$) contribute to the total
116 turbulent sensible and latent heat fluxes ($H_{S,T}$, $H_{L,T}$) at the air-sea interface. That is,

$$H_{S,T} = H_S + H_{S,SP}, \quad (1)$$

$$H_{L,T} = H_L + H_{L,SP}. \quad (2)$$

117 where H_S and H_L are the sensible and latent heat fluxes at the air-sea interface due to the air-sea
118 differences of temperature and humidity. Based on observations of total turbulent heat fluxes and the
119 COARE algorithm (Andreas et al., 2015; Fairall et al., 1996) ~~Based on eddy correlation observations,~~
120 A92 ~~(Andreas, 1989, 1990, 1992; Andreas et al., 2015)~~ integrates the sea spray-mediated sensible and
121 latent heat flux spectrums over initial droplet radius ($Q_S(r_0)$ and $Q_L(r_0)$) to estimate $H_{S,SP}$ and $H_{L,SP}$
122 ~~(details in Appendix A)~~ (details in Appendix A; Andreas, 1989, 1990, 1992; Andreas and Decosmo, 2002).
123 The distributions of $Q_S(r_0)$ and $Q_L(r_0)$ spectrums as functions of initial droplet radius r_0 under
124 various atmosphere and ocean state are shown in Fig. 1, indicating that Q_S and Q_L spectrums are more
125 sensitive to the change of WSP10-10-m wind speed, and less sensitive to other variables, including T02-
126 m air temperature, 2-m relative humidity, ~~sea surface temperature~~ SST, surface air pressure and sea
127 surface salinity.

128 The calculation of $H_{S,SP}$ and $H_{L,SP}$ in A92 ~~requires huge amount of computational time~~ is
129 computationally expensive due to full-size spectral integral (Eqn. A5-A6 of Appendix A), therefore it is
130 difficult to apply A92 directly in coupled modeling systems. A15 (Andreas et al., 2015) developed a fast
131 algorithm by using a single representative droplet radius (details in Appendix B), which was widely
132 adopted in recent ~~regional~~ regional and global coupling systems (Xu et al., 2021b; Liu et al., 2012; Garg
133 et al., 2018; Zhao et al., 2017; Song et al., 2022; Bao et al., 2020). In this study, we apply a 3-node GQ
134 method (details in Appendix C) to develop a new fast algorithm to approximate the full-size spectral
135 integral of A92. Notably, GQ can converge exponentially to the actual integral only for a smooth function,
136 which is the prerequisite for GQ (McClarren, 2018). Since as functions of r_0 , $Q_S(r_0)$ and $Q_L(r_0)$ ~~Q_S~~
137 ~~and Q_L~~ are not smooth (Fig. 1), a data sorting from largest to smallest is required. After sorting, local

138 $Q_S(r_0)$ and $Q_L(r_0)$ become $Q_{S_sort}(m)$ and $Q_{L_sort}(m)$, and then GQ can
 139 be used to estimate the integral of $Q_{S_sort}(m)$ and $Q_{L_sort}(m)$. Note that the independent
 140 variable m is not equivalent to the original r_0 , but only indicates the position. In this way, according to
 141 Appendix C, $m_1=443$, $m_2=251$, $m_3=58$ are three GQ nodes of $Q_{S_sort}(m)$ and $Q_{L_sort}(m)$, and we
 142 can get the corresponding r_0 for local $Q_S(Q_L)$, denoted as $r_{S1}(r_{L1})$, $r_{S2}(r_{L2})$ and $r_{S3}(r_{L3})$.
 143 However, the sorting leads to high complexity of GQ comparable to A92, and the values of $r_{S1}(r_{L1})$,
 144 $r_{S2}(r_{L2})$ and $r_{S3}(r_{L3})$ vary under various atmosphere and ocean environments in the globe. Therefore,
 145 it is necessary to find the general approximate values of $r_{S1}(r_{L1})$, $r_{S2}(r_{L2})$ and $r_{S3}(r_{L3})$ by
 146 global statistical analyses, GQ nodes for Q_{SS} and Q_{LS} to avoid the sorting in application.

147

148 To derive the general approximate values of $r_{S1}(r_{L1})$, $r_{S2}(r_{L2})$ and $r_{S3}(r_{L3})$ GQ nodes, we
 149 calculate the distribution of the sea spray-mediated heat flux spectral following A92, based on the global
 150 daily WSP10, T022-m air temperature, 2-m dewpoint temperature, surface pressure and SWH of ERA5
 151 and OISST from August 1, 2018 to August 31, 2018. Since the sea spray-mediated heat flux is not
 152 sensitive to salinity (Fig. 1e&f) and only monthly observational data is available, the ESA monthly
 153 salinity is applied. The ESA monthly salinity is also applied since the sea spray-mediated heat flux is the
 154 least sensitive to salinity (Fig. 1e&f) and only monthly salinity observation data is available. From the
 155 global spectrums, we sort Q_S and Q_L from largest to smallest to obtain local. The GQ nodes
 156 corresponding to r_0 of the sensible (latent) heat flux after sorting are denoted as r_{S1} , r_{S2} and r_{S3} (r_{L1} ,
 157 r_{L2} and r_{L3}) for every grid point, whose global distribution of occurrence frequency in percentage
 158 is shown in Fig. 2. It is noted that except for that r_{L3} is related to WSP10 (Fig. 2e), all other five nodes
 159 have frequency roughly concentrated at a constant (peak frequency >65% in Fig. 2a, b, d-f; Eqn. 3&4),
 160 while for r_{L3} , there is a 92.53% concentration between 55 and 90 μm (Fig. 2c). And then we found
 161 that r_{L3} (55-90 μm) is related to WSP10 (Fig. S1 in supplementary), so that is thereby we set the
 162 approximate values as

$$r_{S1} = 459.056, r_{S2} = 294.185, r_{S3} = 166.771, \quad (3)$$

$$r_{L1} = 443.914, r_{L2} = 251.0498, \quad (4)$$

$$r_{L3} = \begin{cases} 60.310WSP10^{0.1161}, & WSP10 \geq 2 \text{ m/s} \\ 58.086, & WSP10 < 2 \text{ m/s} \end{cases}, \quad (5)$$

163 where the unit of the radius is micrometer. ~~Afterwards, we don't sort anymore, and~~ directly use Eqn.
 164 ~~3-5 then the 3-node GQ~~ to approximate the full-size spectral integral of A92 ~~without sorting as are~~

$$\int_a^b Q_S(r_0) dr_0 \approx \frac{b-a}{2} \sum_{i=1}^3 \omega_i Q_S(r_{Si}), \quad (6)$$

$$\int_a^b Q_L(r_0) dr_0 \approx \frac{b-a}{2} \sum_{i=1}^3 \omega_i Q_L(r_{Li}). \quad (7)$$

165 Here a and b are the lower and upper limits of r_0 , which are set to $2\mu\text{m}$ and $500\mu\text{m}$ based on Andreas
 166 (1990), and ω_i is the corresponding weight ($\omega_1=\omega_3=0.556$, $\omega_2=0.889$), obtained from Mcclarren
 167 (2018). ~~Thus, we can directly use Eqn. (3-7) to estimate the GQ-based $H_{S,SP}$ and $H_{L,SP}$ approximations,~~
 168 ~~avoiding sorting.~~ The new fast algorithm ~~to~~ for approximations estimate the GQ based of $H_{S,SP}$ and
 169 $H_{L,SP}$ approximations is referred to as SPRAY-GQ hereafter.

170 3.2 CFSv2.0-WW3 Coupling System

171 A coupled system based on Climate Forecast System model version 2.0 (CFSv2.0) and
 172 WAVEWATCH III (WW3) is employed to evaluate and compare the effects of sea spray-mediated heat
 173 flux parameterized by A15 and SPRAY-GQ. The CFSv2.0-WW3 has three components, the Global
 174 Forecast System (GFS; <http://www.emc.ncep.noaa.gov/GFS/doc.php>) as the atmosphere component of
 175 CFSv2.0, the Modular Ocean Model version 4 (MOM4; Griffies et al., 2004) as the ocean component of
 176 CFSv2.0, and the WW3 (WAVEWATCH III Development Group, 2016) as the ocean surface wave
 177 component. The variables between CFSv2.0 and WW3 are interpolated and passed using the Chinese
 178 Community Coupler version 2.0 (C-Coupler2; Liu et al., 2018).

179 The CFSv2.0 is mainly applied for intraseasonal and seasonal prediction (e.g., Saha et al., 2014). The
 180 atmosphere component GFS uses a spectral triangular truncation of 382 waves (T382) in the horizontal,
 181 equivalent to a grid resolution of nearly 35 km, and 64 sigma-pressure hybrid layers in the vertical. The
 182 MOM4 is integrated on a nominal 0.5° horizontal grid with enhanced horizontal resolution to 0.25° in
 183 the tropics, and there are 40 levels in the vertical. The CFSv2.0 initial fields at 00:00 UTC of the first
 184 day for experiments were generated by the real time operational Climate Data Assimilation System

185 (Kalnay et al., 1996), downloaded from the CFSv2.0 official website
186 (<http://nomads.ncep.noaa.gov/pub/data/nccf/com/cfs/prod>). The latitude range of WW3 is 78°S–78°N
187 with a spatial resolution of 1/3°. The initial wave fields ~~are~~ were generated from 10-day simulation
188 starting from rest in a stand-alone WW3 model, forced by ERA5 10-m winds and ice concentration. The
189 open boundary conditions of WW3 ~~are~~ were also obtained by the global simulation of the stand-alone
190 WW3 model.

191 In the coupling system, the WW3 obtains 10-m wind and ocean surface current from CFSv2.0, and
192 then provides wave parameters to CFSv2.0. Several wave-mediated processes, including upper ocean
193 mixing modified by Stokes drift-related processes, air-sea fluxes modified by surface current and Stokes
194 drift, and momentum roughness length, are considered. Details of this system are referred to Shi et al.
195 (2022).

196 A series of numerical experiments is conducted to evaluate the effects of the two fast algorithms
197 parameterizations (A15 and SPRAY-GQ) of sea spray-mediated heat flux on ocean, atmosphere and
198 waves in two 56-day periods, from January 3 to February 28, 2017 and from August 3 to September 28,
199 2018 for boreal winter and boreal summer, respectively. For each period, two sensitivity experiments are
200 carried out. The first is the SPRAY-A15 experiment, in which A15 is used with two-way fully coupling.
201 The second is the SPRAY-GQ experiment, in which SPRAY-GQ fast algorithm parameterization is used
202 instead of A15. In addition, we also carry out another 7-day experiment using A92 (SPRAY-A92) to test
203 the runtime.

204 **4 Results**

206 **4.1 Comparison with A92**

207 Based on the daily global WSP10, T022-m air temperature, 2-m dewpoint temperature, surface
208 pressure and SWH of ERA5, the daily global OISST, and the ESA monthly global salinity, $H_{S,SP}$ and
209 $H_{L,SP}$ from A15, SPRAY-GQ and A92 are calculated (Fig. 3). The computational time for SPRAY-GQ
210 is about the same as that for A15, and about 36 times less than the time for A92. Compared with A92

211 (the black dotted line), A15 (red) overestimates $H_{S,SP}$ for low $H_{S,SP}$ (<50 W/m²) and underestimates
 212 $H_{S,SP}$ for high $H_{S,SP}$ (>50 W/m²) with a root mean square error (RMSE= $\sqrt{\sum_{i=1}^n (\hat{y}_i - y_i)^2 / n}$, \hat{y}_i is A15
 213 value, y_i is A92 value, and n is the total number of grid points) of 3.40 W/m² (Fig. 3a), while A15
 214 shows consistent overestimations with a RMSE of 2.98 W/m² for $H_{L,SP}$ (Fig. 3b). Overall, the RMSE
 215 of A15 is about 2.69 W/m² for sea-spray mediated total heat flux ($TH_{SP} = H_{S,SP} + H_{L,SP}$; Fig. 3c). Andreas
 216 et al. (2015) derived A15 from A92 using single-radius droplets as bellwethers and wind functions, and
 217 extrapolated the wind functions at high wind speeds >25 m/s. Since here the wind speeds in the study are
 218 less than 25 m/s (Fig. S1), the large difference between A15 and A92 is mainly due to the use of single-
 219 radius droplets. Compared with A15, SPRAY-GQ (blue) has less deviation from A92 for both $H_{S,SP}$ and
 220 $H_{L,SP}$ (Fig. 3a&b). The corresponding RMSEs of SPRAY-GQ for $H_{S,SP}$, $H_{L,SP}$ and TH_{SP} are 0.83
 221 W/m², 0.92 W/m² and 0.62 W/m², all significantly lower ($P < 0.05$ in Student's t-test) than those of A15.

222 To test robustness of the results, we also use WSP10, T022-m air temperature and 2-m SPHspecific
 223 humidity of OAFlux dataset to estimate $H_{S,SP}$ and $H_{L,SP}$. As shown in Fig. 4, SPRAY-GQ has
 224 significantly ($P < 0.05$ in Student's t-test) lower deviations and RMSEs than A15, consistent with Fig. 3.
 225 Note that the values of $H_{S,SP}$ and $H_{L,SP}$ in Fig.4 are larger than those in Fig. 3, since the equivalent
 226 neutral wind speed from OAFlux is generally overestimated compared to the observed wind speed
 227 (Seethala et al., 2021; Praveen Kumar et al., 2012). Because it is because OAFlux only provides neutral
 228 wind speeds, calculated from wind stress and the corresponding roughness by assuming air is neutrally
 229 stratified., While previous studies indicated the neutral winds from OAFlux are larger than winds in
 230 ERA5 as indicated by previous studies (Lindemann et al., 2021; Seethala et al., 2021).

231 In addition, since it is common to derive SWH from empirical equations (e.g., Andreas et al., 2008;
 232 Andreas et al., 2015; Andreas and Decosmo, 2002; Andreas, 1992), we also use SWH generated by
 233 empirical equations of WSP10 (Andreas, 1992) instead of ERA5 SWH to estimate $H_{S,SP}$ and $H_{L,SP}$
 234 (Fig. 5). Again, the RMSEs decrease significantly ($P < 0.05$ in Student's t-test) in SPRAY-GQ compared
 235 to A15, though the RMSEs become higher for all estimates due to the enhanced biases of SWH.
 236 Thereby, it is clear that the performance of SPRAY-GQ is always better than A15. The difference
 237 between SPRAY-GQ and A92 is always smaller than that between A15 and A92. Next, we will evaluate
 238 and compare the two fast algorithms in an atmosphere-ocean-wave coupled system (CFSv2.0-WW3).

239 4.2 Comparison in the CFSv2.0-WW3 Coupling System

240 To compare the computational time of different parameterizations in the large-scale modeling system,
241 the runtime of the fully coupled experiments for 7-day forecast is given in Table 1 as an example. It is
242 shown that the runtime is about the same for SPRAY-GQ and SPRAY-A15. Both experiments run about
243 17 times faster than SPRAY-A92.

244 To illustrate the numerical errors of the two fast algorithms discussed in the context of the coupled
245 system~~In this section~~, comparisons are made for simulated SSTs, WSP10s as well as SWHs against
246 OISST and ERA5 reanalysis ~~(Figs. 6-11), to present the numerical errors of the two fast algorithms~~
247 ~~discussed in the context of the coupled system.~~ The results in the first three days are excluded in the
248 comparison, since the wave influences are weak at the beginning of the simulations. Overall, the WSP10s
249 of simulations are generally in the range of 0-25 m/s globally. ~~As shown in Fig. S2&S3 of~~
250 ~~supplementary, At mid-high latitudes, the WSP10s generally can exceed 10 m/s (Fig. S2&S3 of the~~
251 ~~supplementary),; the threshold at which the effects of sea spray can become significant~~ (Andreas et al.,
252 2015; Andreas et al., 2008). ~~Overall, WSP10s of simulations are in the range of 0-25 m/s. Besides, we~~
253 ~~calculate the runtime of the fully coupled experiments with different parameterizations for 7 day forecast~~
254 ~~(Table 1). The runtime computational time is about the same for experiments SPRAY-GQ and SPRAY-~~
255 ~~A15, while the runtime of SPRAY-GQ experiment is about 17 times less than the runtime of SPRAY-~~
256 ~~A92 experiment.~~

257 4.2.1 Sea Surface Temperature (SST)

258 In the austral summer, compared with OISST, large SST biases (>1 °C or <-1 °C) of SPRAY-A15
259 occur in the Southern Hemisphere (SH; Fig. S41a in supplementary), especially in the Southern Ocean.
260 It is always a challenge for reducing the large SST biases in the Southern Ocean for climate models (e.g.,
261 Alessandro et al., 2019; Wang et al., 2014; Li et al., 2013; Bodas-Salcedo et al., 2012; Ceppi et al., 2012).
262 In Fig. 6a, SSTs north (south) of 50°S in experiment SPRAY-A15 are mainly underestimated
263 (overestimated). The domain-averaged RMSE (0-360°E, 40-75°S) increases in the first month and then
264 levels off (red solid line in Fig. 6c). While the domain-averaged RMSE in experiment SPRAY-GQ levels
265 off about a week earlier (black solid line in Fig. 6c). The ~~time series of mean~~ RMSE in SPRAY-GQ is

266 significantly lower than that in SPRAY-A15 ($P < 0.05$ in Student's t-test). The increased (decreased) SSTs
 267 north (south) of 50°S in SPRAY-GQ compared to those in SPRAY-A15 (Fig. 6b) reduce the RMSE of
 268 SST in SPRAY-GQ. And the results of We also calculate the mean absolute error, $(MAE = \sum_{i=1}^n |\hat{y}_i -$
 269 $y_i|/n$, where \hat{y}_i is simulated value and y_i is OISST data, and n is the total number of grid points. The
 270 MAEs) are consistent with RMSEs (dotted line in Fig. 6c). Furthermore, the corresponding positive
 271 mean errors, $(ME = \sum_{i=1}^n (\hat{y}_i - y_i)/n)$ in (-Fig. S5a in the supplementary), indicates the overall
 272 overestimation, which arcs reduced smaller in SPRAY-GQ than SPRAY-A15. The decreased SST
 273 RMSE in SPRAY-GQ is resulted from the increased (decreased) SSTs north (south) of 50°S (Fig. 6b).

274 To understand the effects of sea spray droplets on SST, we calculate the total heat flux ($TH = H_{S,T} + H_{L,T}$)
 275 differences between SPRAY-GQ and SPRAY-A15 (Fig. 42g7a). The TH differences are significantly
 276 correlated with SST differences (Fig. S4b-S4b in the supplementary), with the spatial correlation
 277 coefficient of -0.41 ($P < 0.05$ in Student's t-test). We further decompose direct and indirect effects of sea
 278 spray droplets on heat fluxes following Song et al. (2022). The direct effect ($H_{S,SP}$ and $H_{L,SP}$) is induced
 279 directly by sea spray droplets, calculated from A15 (Eqn. B1-B4 of Appendix B) and SPRAY-GQ
 280 (Section 3.1). The indirect effect (H_S and H_L) is the heat flux variation induced by changes of
 281 atmosphere and ocean variables (including wind, pressure, humidity and temperature) caused by direct
 282 effect, estimated by subtracting $H_{S,SP}$ and $H_{L,SP}$ from the output heat fluxes ($H_{S,T}$ and $H_{L,T}$) of
 283 experiment SPRAY-A15 and SPRAY-GQ.

284 In the Southern Ocean, although direct differences of $H_{S,SP}$ and $H_{L,SP}$ are relatively small (< 10
 285 W/m^2 , Fig. 42b7b, e, & h), the resulting changes of temperature and humidity lead to relatively large
 286 differences in indirect effects of H_S and H_L (Fig. 42e7c, f, & i). Enhanced (reduced) $TH_{S,SP}$ from ocean
 287 to atmosphere in the summer leads to increased (decreased) air-sea temperature difference and thus
 288 enhances (weakens) H_S . Meanwhile the warmer (cooler) air also causes more (less) evaporation and thus
 289 more (less) H_L . Finally, the enhanced (reduced) TH cools (warms) SST.

290 In the boreal summer, large SST biases (> 1 °C or < -1 °C) of SPRAY-A15 mainly occur at mid-high
 291 latitudes of the Northern Hemisphere (NH; Fig. S2a-S6a in supplementary). Significant underestimations
 292 occur in the western and northern part of the North Pacific and at mid latitudes of the North Atlantic,
 293 while large positive SST biases mainly occur in the eastern part of the North Pacific and at high latitudes

294 of the North Atlantic (Fig. 7a8a). In experiment SPRAY-GQ, SSTs are warmer (cooler) in the previously
295 underestimated (overestimated) regions (Fig. 7b8b). Therefore, the domain-averaged RMSE and MAE
296 (0-360°E, 20-75°N) in SPRAY-GQ ~~is are~~ significantly lower ($P < 0.01$ in Student's t-test) than in SPRAY-
297 A15 after the first three weeks (Fig. 7e8c). Compared to And SPRAY-A15, the overall underestimation
298 is reduced in SPRAY-GQ than SPRAY-A15 (Fig. S5b). The spatial correlation coefficient between TH
299 differences and SST differences (Fig. 13e9a&Fig. S2bS6b) is -0.32 ($P < 0.05$ in Student's t-test).
300 Consistent with the austral summer, the SST changes are related to the changes of heat flux (Fig. 139).
301 The indirect effects of latent heat flux (Fig. 13e9f) play a major role in TH differences, which are
302 modified by the direct effects (Fig. 13b9b, e, &h). In addition, the changes of surface wind also contribute
303 to the changes of SST. ~~The enhanced (reduced) winds lead to stronger (weaker) ocean mixing, and thus~~
304 ~~cooler (warmer) SST (Fig. S3&S4).~~ The reduced winds weaken the upper ocean mixing, so the water
305 becomes more stratified, and then the SST tends to be warmer, and vice versa (Fig. S7&S8).

306 4.2.2 10-m Wind Speed (WSP10) and Significant Wave Height (SWH)

307 Compared with experiment SPRAY-A15, significant ~~improvements~~ differences of WSP10 in SPRAY-
308 GQ occur at mid-low latitudes of the NH (0-360°E, 0-60°N) in both winter and summer
309 (Fig. S7b8&S8b9). As we know, satellite scatterometer and altimeter data are usually used to validate
310 WSP10 and SWH for short term weather forecast (e.g., Accadia et al., 2007; Djurdjevic and Rajkovic,
311 2008; Myslenkov et al., 2021). ~~However, due to the spatial and temporal limitations~~ coverage of satellite
312 data, we can only obtain the monthly averaged satellite data for the globe. So we compare the monthly
313 differences of averaged WSP10 and SWH from simulations over the periods between simulations
314 and with the corresponding satellite data (Fig. S9-S12). The average WSP10 and SWH differences
315 compared with satellite data comparison results (Fig. S9a&c-S12a&c) are consistent with those compared
316 with ERA5 (Fig. S9b&d-S12b&d). From Fig. S9e-S12e, Besides, the differences domain averaged
317 RMSEs of WSP10s between ERA5 and the satellite data are always less than 1 m/s and are 0.48 m/s,
318 0.53 m/s, 0.15 m and 0.12 m (Fig. S9e-S12e the differences of). SWHs are always less than 0.3 m. Since
319 ERA5 provides daily data for comparison and the differences between ERA5 and satellite data are small,
320 we will use ERA5 to validate simulations for validation in the following.

321 The ~~domain-averaged bias~~ME of WSP10 (SPRAY-A15 minus ERA5) is 0.~~37-28~~ m/s and 0.~~24-47~~ m/s
 322 in winter and summer (~~red in Fig. S5c&d~~), respectively, mainly due to the overestimations over the
 323 Pacific and the Atlantic Ocean (~~red in Fig. 108a&119a~~). Whereas in SPRAY-GQ, the ~~domain-averaged~~
 324 ~~bias~~ME (SPRAY-GQ minus ERA5) is 0.~~26-15~~ m/s and 0.~~03-33~~ m/s in winter and summer respectively
 325 (~~black in Fig. S5c&d~~). The domain-averaged RMSEs and MAEs of WSP10s increase with time in the
 326 first two weeks and then gradually level off (Fig. ~~108c&119c~~). The differences of WSP10 RMSEs and
 327 MAEs between SPRAY-GQ (black) and SPRAY-A15 (red) are very small in the first two weeks.
 328 Afterwards the mean values of time-series-of-RMSE and MAE in SPRAY-GQ ~~is-are~~ lower than ~~that-those~~
 329 in SPRAY-A15 significantly at ~~95~~9% confidence level in both boreal winter (Fig. ~~8e10c~~) and boreal
 330 summer (Fig. ~~119c~~).

331 The simulated SWHs changes are closely related to the changes of WSP10s (Shi et al., 2022).
 332 Therefore, the differences of SWHs (Fig. ~~120&134~~) are consistent with those of WSP10s (Fig. ~~108&119~~),
 333 with overestimated (underestimated) WSP10s corresponding to overestimated (underestimated) SWHs
 334 compared with ERA5. The SWHs in SPRAY-GQ show are significantly differences with those in
 335 SPRAY-A15~~The SWHs in SPRAY-GQ improve compared with those in SPRAY-A15~~ (Fig.
 336 ~~10b12b&134b~~), especially in summer. In winter (summer), the SWH RMSE averages for SPRAY-A15
 337 and SPRAY-GQ are 1.31 m (0.98 m) and 1.23 m (0.87 m), and after the first two weeks the -time-series
 338 of-RMSE and MAE in SPRAY-GQ ~~is-are~~ lower than ~~that-those~~ in SPRAY-A15 significantly at ~~95~~9%
 339 confidence level in both winter (Fig. ~~10e12c~~) and summer (Fig. ~~11e13c~~).

340 The direct and indirect effects of sea spray droplets on heat fluxes can influence estimates of WSP10
 341 and then SWH. The changes of WSP10s are related to the direct effects ($H_{S,SP}$ and $H_{L,SP}$; Fig. ~~12b7b~~, e,
 342 &h; Fig. ~~13b9b~~, e, &h). The spatial correlation coefficients between WSP10 differences (Fig.
 343 ~~S3bS7b&S4bS8b~~) and TH_{SP} differences (Fig. ~~12h7b&13h9b~~) are 0.51 and 0.69 ($P < 0.01$ in Student's t-
 344 test) in winter and summer, respectively. Because TH_{SP} differences can influence the sea level pressure
 345 (SLP) distribution (Fig. S15&S16), and thus influences subsequently surface winds. For example,
 346 compared with SPRAY-A15, the decreased TH_{SP} of SPRAY-GQ in the Northwest Pacific in summer
 347 (Fig. 9b) leads to higher SLP and smaller pressure gradient (Fig. S16), and thus decreased WSP10 (Fig.
 348 11b); while the increased TH_{SP} in the Gulf of Alaska (Fig. 9b) leads to lower SLP and larger pressure

349 ~~gradient (Fig. S16), and thus enhanced WSP10 (Fig. 11b), the directly increased (decreased) heat fluxes~~
350 ~~enhance (reduce) turbulence, promote (hinder) the downward transmission of momentum from the upper~~
351 ~~layer of atmosphere, and then accelerate (decelerate) the surface wind speed (Wallace et al., 1989). While~~
352 ~~the accelerated (decelerated) WSP10s further result in increased (decreased) interfacial heat transport~~
353 ~~(H_S , H_L), as well as increased (decreased) SWHs.~~

354 **5 Conclusions and Discussions**

355 Based on a GQ method, we develop a new fast algorithm based on Andreas's (1989, 1990, 1992) full-
356 size microphysical parameterization (A92) for sea spray-mediated heat fluxes. Using global satellite
357 measurements and reanalysis data, ~~we found that the difference between SPRAY-GQ and A92 is~~
358 ~~significantly smaller than that between A15 and A92~~~~SPRAY-GQ parameterization is validated to~~
359 ~~approximate A92 more accurately than the A15 fast algorithm~~ (Andreas et al., 2015). To evaluate the
360 ~~numerical error of SPRAY-GQ/A15 fast algorithm parameterization~~, we implement them in the two-way
361 coupled CFSv2.0-WW3 system. A series of 56-day simulations from January 3 to February 28, 2017 and
362 from August 3 to September 28, 2018 are conducted. The results are compared against ~~QISST~~ satellite
363 measurements and ERA5 reanalysis. The comparison shows that the sea spray-mediated heat flux in
364 SPRAY-GQ can reasonably modulate total heat flux ~~compared with SPRAY-A15, and significantly~~
365 ~~improve-reduce~~ the SST biases in the Southern Ocean (mid-high latitudes of the NH) for the austral
366 (boreal) summer, as well as WSP10 and SWH ~~after the first two weeks~~ at mid-low latitudes of the NH
367 for both boreal winter and summer. Overall, our fast algorithm based on GQ is applicable to sea spray-
368 mediated heat flux parameterization in coupled models.

369 ~~To investigate the effects of spray-mediated heat flux on simulations, two 56-day experiments without~~
370 ~~sea spray effect (CTRL) in boreal winter summer and summer respectively winter are conducted~~~~added,~~
371 ~~and the differences of simulated SST, WSP10, SWH, T02 and SPH between SPRAY-GQ and CTRL are~~
372 ~~compared in Fig. S17-S21 in the supplementary. The introduction of sea spray cannot significantly~~
373 ~~reduce the global overall errors of simulations, but it leads to regional improvements (blue in Fig.~~
374 ~~S17e&f-S21e&f). For example, compared with CTRL in Jan-Feb, 2017, SST MAE of SPRAY-GQ in~~
375 ~~the southeast of Australia decreases (Fig. S17e), because of warmer SST (Fig. S17c) related to reduced~~

376 wind (Fig. S18c). The reduced wind here also leads to lower SWH (Fig. S19c) and thus reduced SWH
377 overestimation (Fig. S19e). Meanwhile, T02 and SPH in CTRL are underestimated in this area (Fig.
378 S20a&S21a), while SPRAY-GQ reduces decreases MAE of T02 and SPH (Fig. S20e&S21e) by
379 increasing temperature and moisture (Fig. S20c&S21c). Besides, †The reduced errors are related to the
380 relatively large WSP10s over the corresponding areas (Fig. S2&S3), since the effects of sea spray become
381 significantimportant at wind speeds larger than 10 m/s.

382 In addition to the variables aforementioned, the changes of simulated cloud fraction were also
383 compared. However, the effects of sea spray-mediated heat flux on cloud fraction are non-significant for
384 the 2-month simulation, so the results are not shown. Besides, the lack of other processes related to sea
385 spray may be one of reasons why the global overall error cannot be reduced effectively. For example, for
386 simulated WSP10 and SWH in SPRAY-GQ, the SPRAY-GQ parameterization used in the study mainly
387 improves the biases at mid-low latitudes of the NH, while the significant overestimations in the SH are
388 only slightly improvedstill exist especially in Aug-Sep, 2018 (Fig. S3S18&-S196 in supplementary). As
389 Andreas (2004) indicated, sea spray droplets also influence the surface momentum flux by injecting more
390 momentum into the ocean from the atmosphere, which might further decrease the surface wind speed.
391 We will consider this process in the future study.

392 Sea spray-mediated heat fluxes are sensitive torelated to the sea spray generation function
393 (SSGF) dF/dr_g . Based on a number of laboratory and field observations, varieties of $SSGF dF/dr_g$
394 were derived (e.g., Koga, 1981; Monahan et al., 1982; Troitskaya et al., 2018; Andreas, 1992, 1998, 2002;
395 Fairall et al., 1994; Veron, 2015), whereas their differences can reach six orders of magnitude (Andreas,
396 1998). There is currently no consensus on the most suitable choice. In this study, we use $SSGF dF/dr_g$
397 of Fairall et al. (1994), recommended by Andreas (2002), to get a mean bias of 3.70 W/m² and 0.095
398 W/m² for latent and sensible heat flux respectively (Andreas et al., 2015). It is also, consistent with recent
399 observations of Xu et al. (2021a). (Andreas et al., 2015)Since the new scheme based on GQ is
400 independent of sea spray generation function, the new scheme can also be applied to sea spray mediated
401 heat fluxes estimation with different dF/dr_g . Besides, considering the uncertainty of SSGF, the sea
402 spray mediated heat fluxes in A92 have been tuned by non-negative constants based on observations and
403 the COARE algorithm to reduce the uncertainties (Andreas and Decosmo, 2002; Andreas et al., 2008;

404 Andreas et al., 2015; Andreas, 2003). In this study, we use the constants (Eqn. A7 A8 in Appendix A)
405 for the SSGF (Fairall et al., 1994) to get a mean bias of 3.70 and 0.095 W/m² for latent and sensible heat
406 flux respectively in A92 compared to observations (Andreas et al., 2015). Therefore, a few W/m²
407 improvements of numerical errors in this study are relevant. Even though, the improved SST and other
408 variables cannot be reliably assigned to the usage of the GQ method, due to the uncertainties of the
409 coupled model itself and SSGF.

410 When wind speed is larger than 10 m/s, spray-mediated heat flux can become as important as the
411 interfacial heat flux (Andreas and Decosmo, 1999, 2002). Particularly, even in the absence of air-sea
412 temperature difference, the spray-mediated sensible heat flux is still present (Andreas et al., 2008). As
413 indicated by previous studies (e.g., Garg et al., 2018; Song et al. 2022), it is necessary to superimpose
414 the spray-mediated heat flux on the bulk formula to complete the physics of turbulent heat transfer for
415 coupled simulation. Since the full microphysical parameterization (A92) is computationally expensive,
416 an efficient algorithm that captures the main features of A92 can be beneficial to large-scale climate
417 systems or operational storm models. The GQ method proposed in the study can efficiently calculate the
418 spray-mediated heat flux, and agree better with A92 than A15. Thereby, ~~Thus,~~ the GQ based spray-
419 mediated heat flux ~~method has a great potential to~~ is promising to be widely applied in large-scale climate
420 systems and operational storm models.

421

422 **Appendix A**

423 **Microphysical Parameterization of A92**

424 Based on the cloud microphysical parameterization of Pruppacher and Klett (1978), Andreas (1989,
425 1990, 1992) proposed a parameterization of sea spray-related heat fluxes for droplets with different radius,
426 from formation at sea surface to equilibrium with environment, that is,

$$Q_S = \rho_w C_{ps} (T_w - T_{eq}) \left[1 - \exp\left(-\frac{\tau_f}{\tau_T}\right) \right] \left(\frac{4\pi r_0^3}{3} \frac{dF}{dr_0} \right), \quad (\text{A1})$$

$$Q_L = \begin{cases} \rho_w L_v \left\{ 1 - \left[\frac{r(\tau_f)}{r_0} \right]^3 \right\} \left(\frac{4\pi r_0^3}{3} \frac{dF}{dr_0} \right), \tau_f \leq \tau_r, \\ \rho_w L_v \left\{ 1 - \left(\frac{r_{eq}}{r_0} \right)^3 \right\} \left(\frac{4\pi r_0^3}{3} \frac{dF}{dr_0} \right), \tau_f > \tau_r. \end{cases} \quad (A2)$$

427 Here Q_S , Q_L are sensible heat flux and latent heat flux resulted by sea spray droplets with initial radius
 428 r_0 , ρ_w is the sea water density, C_{ps} is the specific heat, L_v is the latent heat of vaporization of water,
 429 T_w is the water temperature, T_{eq} is the temperature of droplet when it reaches thermal equilibrium with
 430 ambient condition, r_{eq} is the radius of droplet when it reaches moisture equilibrium with ambient
 431 condition, τ_f is the residence time for droplets in the atmospheric, $r(\tau_f)$ is the corresponding radius,
 432 τ_T is the characteristic e-folding time of droplet temperature, and τ_r is the characteristic e-folding time
 433 of droplet radius. The detailed calculation of these microphysical quantities can be found in Andreas
 434 (1989, 1990, 1992). And dF/dr_0 is the sea spray generation function, which represents the number
 435 produced of droplets with initial radius r_0 (Andreas, 1992). For this term, the function of Fairall et al.
 436 (1994) was recommended by Andreas (2002). According to the review in Andreas (2002), the dF/dr_0
 437 of Fairall et al. (1994) is related on that of Andreas (1992) as

$$\frac{dF}{dr_0} = 38 \times 3.84 \times 10^{-6} U_{10}^{3.41} r_0^{-0.024} \left. \frac{dF_{A92}}{dr_{80}} \right|_{U_{10}=11 \text{ m/s}}, \quad (A3)$$

$$\left. \frac{dF_{A92}}{dr_{80}} \right|_{U_{10}=11 \text{ m/s}} = \begin{cases} e^{(4.405-2.646(\log r_{80})-3.156(\log r_{80})^2+8.902(\log r_{80})^3-4.482(\log r_{80})^4)}, r_{80} \leq 15 \mu\text{m}; \\ 1.02 \times 10^4 r_{80}^{-1}, 15 \leq r_{80} \leq 37.5 \mu\text{m}; \\ 6.95 \times 10^6 r_{80}^{-2.8}, 37.5 \leq r_{80} \leq 100 \mu\text{m}; \\ 1.75 \times 10^{17} r_{80}^{-8}, r_{80} \geq 100 \mu\text{m} \end{cases} \quad (A4)$$

438 Here U_{10} is the 10-m wind, $r_{80} = 0.518r_0^{0.976}$.

439 The total sea spray fluxes are obtained by integrating Q_S and Q_L corresponding to all r_0 . Based on
 440 Andreas (1990), the lower and upper limits of r_0 is $2\mu\text{m}$ and $500\mu\text{m}$, that is,

$$\overline{Q_S} = \int_2^{500} Q_S(r_0) dr, \quad (A5)$$

$$\overline{Q_L} = \int_2^{500} Q_L(r_0) dr. \quad (A6)$$

441 While $\overline{Q_S}$ and $\overline{Q_L}$ are nominal sea spray fluxes but not the actual $H_{S,SP}$ and $H_{L,SP}$ (Andreas and
 442 Decosmo, 1999, 2002), because there are interactions between these two terms and the microphysical
 443 functions also lead to uncertainties (Fairall et al., 1994). Therefore, $\overline{Q_S}$ and $\overline{Q_L}$ are tuned by non-
 444 negative constants α , β and γ (Andreas and Decosmo, 2002; Andreas et al., 2008; Andreas et al., 2015;
 445 Andreas, 2003) as

$$H_{S,SP} = \beta \overline{Q_S} - (\alpha - \gamma) \overline{Q_L}, \quad (A7)$$

$$H_{L,SP} = \alpha \overline{Q_L}. \quad (A8)$$

446 In Eqn. (A8), the α term indicates the sea spray-mediated latent heat flux from the top of DEL to
 447 atmosphere. Because the evaporation of droplets absorbs heat, which is provided by sea spray-mediated
 448 sensible heat (Fairall et al., 1994), the negative α term appears in Eqn. (A7). Whereas the evaporation
 449 also cools DEL and thus increases the air-sea temperature difference, therefore it contributes to a positive
 450 γ term in Eqn. (A7). Different values of α , β and γ were given in Andreas and Decosmo (2002),
 451 Andreas (2003), Andreas et al. (2008) and Andreas et al. (2015), to minimize the bias between
 452 estimations and observations of turbulent heat fluxes measured by eddy correlation. And Andreas et al.
 453 (2015) validated the most observation data, which are 4000 sets, to derive $\alpha = 2.46, \beta = 15.15, \gamma =$
 454 1.77 .

455 Appendix B

456 Fast Algorithm of A15

457 Andreas (2003) and Andreas et al. (2008, 2015) developed a fast algorithm to approximate $H_{S,SP}$,
 458 $H_{L,SP}$ by a characteristic radius, that is,

$$H_{S,SP} = \beta \overline{Q_S} - (\alpha - \gamma) \overline{Q_L} \approx \rho_w C_{ps} (T_W - T_{eq,100}) V_S(u_*), \quad (B1)$$

$$H_{L,SP} = \alpha \overline{Q_L} \approx \rho_w L_v \left\{ 1 - \left[\frac{r(\tau_{f,50})}{50 \mu\text{m}} \right]^3 \right\} V_L(u_*). \quad (B2)$$

459 Here $T_{eq,100}$ is T_{eq} of droplets with $r_0=100 \mu\text{m}$, $\tau_{f,50}$ is τ_f of droplets with $r_0=50 \mu\text{m}$, V_S and
 460 V_L are functions of the bulk friction velocity u_* . As indicated by Andreas et al. (2008, 2015), the
 461 characteristic radiuses of $100 \mu\text{m}$ and $50 \mu\text{m}$ for sensible and latent heat fluxes are chosen,
 462 respectively, because Q_S and Q_L show a large peak in the vicinity of these values (Fig. 1). V_S and V_L
 463 are calculated in Andreas et al. (2015) as

$$V_S = \begin{cases} 3.92 \times 10^{-8}, & 0 \leq u_* \leq 0.1480 \text{ m/s} \\ 5.02 \times 10^{-6} u_*^{2.54}, & u_* \geq 0.1480 \text{ m/s} \end{cases} \quad (B3)$$

$$V_L = \begin{cases} 1.76 \times 10^{-9}, & 0 \leq u_* \leq 0.1358 \text{ m/s} \\ 2.08 \times 10^{-7} u_*^{2.39}, & u_* \geq 0.1358 \text{ m/s} \end{cases} \quad (B4)$$

464 **Appendix C**

465 **Gaussian Quadrature (GQ)**

466 GQ is a method to approximate the definite integral of a function $f(x)$ via the function values at a
467 small number of specified nodes (Gauss, 1815; Jacobi, 1826). In this study we use the form of n-node
468 Gauss–Legendre quadrature on $[-1, 1]$ as

$$\int_{-1}^1 f(x) dx \approx \sum_{i=1}^n \omega_i f(x_i). \quad (C1)$$

469 Here x_i is the specified node, and ω_i is the corresponding weight. For $n=3$, $x_1=-0.775$, $x_2=0$,
470 $x_3=0.775$, $\omega_1=\omega_3=0.556$, $\omega_2=0.889$.

471 While for a function $g(\xi)$ on $[a, b]$, Eqn. (C1) can be transformed to

$$\begin{aligned} \int_a^b g(\xi) d\xi &= \int_{-1}^1 g\left(\frac{b-a}{2}x + \frac{a+b}{2}\right) \frac{d\xi}{dx} dx \\ &\approx \frac{b-a}{2} \sum_{i=1}^n \omega_i g\left(\frac{b-a}{2}x_i + \frac{a+b}{2}\right). \end{aligned} \quad (C2)$$

472 **Code and data availability**

473 The code of sea spray can be found under <https://doi.org/10.5281/zenodo.7100345> or
474 <https://zenodo.org/record/7100345#.Y66vRtVByHt> (Shi and Xu, 2022). The code for CFSv2.0-WW3
475 system can be found under <https://doi.org/10.5281/zenodo.5811002> (Shi et al., 2021) including the
476 coupling, preprocessing, run control and postprocessing scripts. The initial fields for CFSv2.0 are
477 generated by the real time operational Climate Data Assimilation System, downloaded from the CFSv2.0
478 official website (<http://nomads.ncep.noaa.gov/pub/data/nccf/com/cfs/prod>). The daily average satellite
479 Optimum Interpolation SST (OISST) data are obtained from NOAA (<https://www.ncdc.noaa.gov/oisst>).
480 The fifth generation European Centre for Medium-Range Weather Forecasts (ECMWF) Reanalysis
481 (ERA5) are available at the Copernicus Climate Change Service (C3S) Climate Data Store
482 (<https://cds.climate.copernicus.eu/cdsapp#!/dataset/reanalysis-era5-single-levels>). The daily Objectively
483 Analyzed air-sea Fluxes (OAFflux) products are available at <https://oafux.whoi.edu/heat-flux>. The global
484 monthly mean salinity observations of European Space Agency (ESA) are from <https://climate.esa.int>.
485 [The monthly global ocean RSS Satellite Data Products for 10-m wind speed are from](#)
486 https://data.remss.com/wind/monthly_1deg/, and the [Reprocessed L4 Satellite Measurements for](#)

487 [significant wave height are from https://doi.org/10.48670/moi-00177](https://doi.org/10.48670/moi-00177).

488 **Author contribution**

489 FX and RS designed the experiments and RS carried them out. RS developed the code of coupling
490 parametrizations and produced the figures. RS prepared the manuscript with contributions from all co-
491 authors. FX contributed to review and editing.

492 **Acknowledgments**

493 This work was supported by the National Key Research and Development Program of China
494 (2020YFA0607900, 2021YFC3101601), and the National Natural Science Foundation of China
495 (42176019). We ~~also~~ thank Dr. Jiangnan Li for help of GQ codes. [We also thank two anonymous
496 reviewers and the handling editor for their constructive comments.](#)

497 **Competing Interests**

498 The contact author has declared that neither they nor their co-authors have any competing interests.

499 **References**

500 Accadia, C., Zecchetto, S., Lavagnini, A., and Speranza, A.: Comparison of 10-m wind forecasts from a
501 regional area model and QuikSCAT scatterometer wind observations over the Mediterranean Sea, Mon.
502 Weather Rev., 135, 1945-1960, 2007.

503 Alessandro, J. D., Diao, M., Wu, C., Liu, X., Jensen, J. B., and Stephens, B. B.: Cloud phase and relative
504 humidity distributions over the Southern Ocean in austral summer based on in situ observations and
505 CAM5 simulations, Journal of Climate, 32, 2781-2805, 2019.

506 Andreas, E. L.: Thermal and size evolution of sea spray droplets, 1989.

507 Andreas, E. L.: Time constants for the evolution of sea spray droplets, Tellus B, 42, 481-497, 1990.

508 Andreas, E. L.: Sea spray and the turbulent air - sea heat fluxes, Journal of Geophysical Research:
509 Oceans, 97, 11429-11441, 1992.

510 Andreas, E. L.: A new sea spray generation function for wind speeds up to 32 ms⁻¹, Journal of Physical

511 Oceanography, 28, 2175-2184, 1998.

512 Andreas, E. L.: A review of the sea spray generation function for the open ocean, *Advances in Fluid*
513 *Mechanics*, 33, 1-46, 2002.

514 Andreas, E. L.: 3.4 AN ALGORITHM TO PREDICT THE TURBULENT AIR-SEA FLUXES IN
515 HIGH-WIND, SPRAY CONDITIONS, 2003.

516 Andreas, E. L.: Spray stress revisited, *Journal of physical oceanography*, 34, 1429-1440, 2004.

517 Andreas, E. L.: Spray-mediated enthalpy flux to the atmosphere and salt flux to the ocean in high winds,
518 *Journal of physical oceanography*, 40, 608-619, 2010.

519 Andreas, E. L. and Decosmo, J.: Sea spray production and influence on air-sea heat and moisture fluxes
520 over the open ocean, in: *Air-sea exchange: physics, chemistry and dynamics*, Springer, 327-362, 1999.

521 Andreas, E. L. and Decosmo, J.: The signature of sea spray in the HEXOS turbulent heat flux data,
522 *Boundary-layer meteorology*, 103, 303-333, 2002.

523 Andreas, E. L. and Emanuel, K. A.: Effects of sea spray on tropical cyclone intensity, *Journal of the*
524 *atmospheric sciences*, 58, 3741-3751, 2001.

525 Andreas, E. L., Mahrt, L., and Vickers, D.: An improved bulk air - sea surface flux algorithm, including
526 spray - mediated transfer, *Quarterly Journal of the Royal Meteorological Society*, 141, 642-654, 2015.

527 Andreas, E. L., Persson, P. O. G., and Hare, J. E.: A bulk turbulent air-sea flux algorithm for high-wind,
528 spray conditions, *Journal of Physical Oceanography*, 38, 1581-1596, 2008.

529 Andreas, E. L., Edson, J. B., Monahan, E. C., Rouault, M. P., and Smith, S. D.: The spray contribution
530 to net evaporation from the sea: A review of recent progress, *Boundary-Layer Meteorology*, 72, 3-52,
531 1995.

532 Bao, Y., Song, Z., and Qiao, F.: FIO - ESM version 2.0: Model description and evaluation, *Journal of*
533 *Geophysical Research: Oceans*, 125, e2019JC016036, 2020.

534 Bodas-Salcedo, A., Williams, K., Field, P., and Lock, A.: The surface downwelling solar radiation
535 surplus over the Southern Ocean in the Met Office model: The role of midlatitude cyclone clouds, *Journal*
536 *of Climate*, 25, 7467-7486, 2012.

537 Borisenkov, E.: Some mechanisms of atmosphere-ocean interaction under stormy weather conditions,
538 *Probl Arct Antarct*, 43, 73-83, 1974.

539 Bortkovskii, R.: On the mechanism of interaction between the ocean and the atmosphere during a storm,
540 Fluid Mech Sov Res, 2, 87-94, 1973.

541 Burk, S. D.: The generation, turbulent transfer and deposition of the sea-salt aerosol, Journal of
542 Atmospheric Sciences, 41, 3040-3051, 1984.

543 Ceppi, P., Hwang, Y. T., Frierson, D. M., and Hartmann, D. L.: Southern Hemisphere jet latitude biases
544 in CMIP5 models linked to shortwave cloud forcing, Geophysical Research Letters, 39, 2012.

545 Djurdjevic, V. and Rajkovic, B.: Verification of a coupled atmosphere-ocean model using satellite
546 observations over the Adriatic Sea, Annales Geophysicae, 1935-1954,

547 Edson, J. B. and Andreas, E. L.: Modeling the role of sea spray on air-sea heat and moisture exchange,
548 Final Rep, 6, 18, 1997.

549 Emanuel, K. A.: Sensitivity of tropical cyclones to surface exchange coefficients and a revised steady-
550 state model incorporating eye dynamics, Journal of Atmospheric Sciences, 52, 3969-3976, 1995.

551 Fairall, C. and Larsen, S. E.: Dry deposition, surface production and dynamics of aerosols in the marine
552 boundary layer, Atmospheric Environment (1967), 18, 69-77, 1984.

553 Fairall, C., Davidson, K., and Schacher, G.: An analysis of the surface production of sea - salt aerosols,
554 Tellus B, 35, 31-39, 1983.

555 Fairall, C., Kepert, J., and Holland, G.: The effect of sea spray on surface energy transports over the
556 ocean, Global Atmos. Ocean Syst, 2, 121-142, 1994.

557 Fairall, C., Bradley, E. F., Rogers, D. P., Edson, J. B., and Young, G. S.: Bulk parameterization of air -
558 sea fluxes for tropical ocean - global atmosphere coupled - ocean atmosphere response experiment,
559 Journal of Geophysical Research: Oceans, 101, 3747-3764, 1996.

560 Fox-Kemper, B., Johnson, L., and Qiao, F.: Ocean near-surface layers, in: Ocean Mixing, Elsevier, 65-
561 94, 2022.

562 Garg, N., Ng, E. Y. K., and Narasimalu, S.: The effects of sea spray and atmosphere-wave coupling on
563 air-sea exchange during a tropical cyclone, Atmospheric Chemistry and Physics, 18, 6001-6021, 2018.

564 Gauss, C. F.: Methodvs nova integralivm valores per approximationem inveniendi, apvd Henricvm
565 Dieterich1815.

566 Griffies, S. M., Harrison, M. J., Pacanowski, R. C., and Rosati, A.: A technical guide to MOM4, GFDL

567 Ocean Group Tech. Rep, 5, 342, 2004.

568 [WAVEWATCH III Development Group, W. I. D.](#): User manual and system documentation of
569 WAVEWATCH III version 5.16, NOAA/NWS/NCEP/MMAB Technical Note 329, 326, 2016.

570 Hersbach, H., Bell, B., Berrisford, P., Hirahara, S., Horányi, A., Muñoz - Sabater, J., Nicolas, J., Peubey,
571 C., Radu, R., and Schepers, D.: The ERA5 global reanalysis, Quarterly Journal of the Royal
572 Meteorological Society, 146, 1999-2049, 2020.

573 Jacobi, C. G. J.: Ueber Gauss neue Methode, die Werthe der Integrale näherungsweise zu finden, 1826.

574 Kalnay, E., Kanamitsu, M., Kistler, R., Collins, W. D., Deaven, D. G., Gandin, L. S., Iredell, M. D., Saha,
575 S., White, G. H., and Woollen, J.: The NCEP/NCAR 40-Year Reanalysis Project, Bulletin of the
576 American Meteorological Society, 77, 437-471, [http://dx.doi.org/10.1175/1520-0477\(1996\)077%3C0437:TNYRP%3E2.0.CO;2](http://dx.doi.org/10.1175/1520-0477(1996)077%3C0437:TNYRP%3E2.0.CO;2), 1996.

577

578 Koga, M.: Direct production of droplets from breaking wind - waves—its observation by a multi -
579 colored overlapping exposure photographing technique, Tellus, 33, 552-563, 1981.

580 Lhuissier, H. and Villiermaux, E.: Bursting bubble aerosols, Journal of Fluid Mechanics, 696, 5-44, 2012.

581 Li, J., Waliser, D., Stephens, G., Lee, S., L'Ecuyer, T., Kato, S., Loeb, N., and Ma, H. Y.: Characterizing
582 and understanding radiation budget biases in CMIP3/CMIP5 GCMs, contemporary GCM, and reanalysis,
583 Journal of Geophysical Research: Atmospheres, 118, 8166-8184, 2013.

584 Li, J. N. and Barker, H. W.: Computation of domain - average radiative flux profiles using Gaussian
585 quadrature, Quarterly Journal of the Royal Meteorological Society, 144, 720-734, 2018.

586 Lindemann, D., Avila-Diaz, A., Pezzi, L., Rodrigues, J., Freitas, R. A., Coelho, L., Alonso, M., and
587 Cerón, W. L.: The Surface Wind Influence on the Heat Fluxes Variability on the South Atlantic, 2021.

588 Ling, S. and Kao, T.: Parameterization of the moisture and heat transfer process over the ocean under
589 whitecap sea states, Journal of Physical Oceanography, 6, 306-315, 1976.

590 Liu, B., Guan, C., Xie, L. a., and Zhao, D.: An investigation of the effects of wave state and sea spray on
591 an idealized typhoon using an air-sea coupled modeling system, Advances in Atmospheric Sciences, 29,
592 391-406, 2012.

593 Liu, L., Zhang, C., Li, R., and Wang, B.: C-Coupler2: a flexible and user-friendly community coupler
594 for model coupling and nesting, Geoscientific Model Development Discussions, 11, 1-63,

595 <http://dx.doi.org/10.5194/gmd-11-3557-2018>, 2018.

596 McClarren, R.: Gauss Quadrature and Multi-dimensional Integrals, Computational Nuclear Engineering
597 and Radiological Science Using Python; Academic Press: Cambridge, MA, USA, 287-299, 2018.

598 Melville, W. K.: The role of surface-wave breaking in air-sea interaction, 1996.

599 Monahan, E. and Van Patten, M. A.: The climate and health implications of bubble-mediated sea-air
600 exchange, 1988.

601 Monahan, E., Davidson, K., and Spiel, D.: Whitecap aerosol productivity deduced from simulation tank
602 measurements, *Journal of Geophysical Research: Oceans*, 87, 8898-8904, 1982.

603 Myslenkov, S., Zelenko, A., Resnyanskii, Y., Arkhipkin, V., and Silvestrova, K.: Quality of the Wind
604 Wave Forecast in the Black Sea Including Storm Wave Analysis, *Sustainability*, 13, 13099, 2021.

605 Praveen Kumar, B., Vialard, J., Lengaigne, M., Murty, V., and Mcphaden, M. J.: TropFlux: Air-sea
606 fluxes for the global tropical oceans—Description and evaluation, *Climate dynamics*, 38, 1521-1543,
607 2012.

608 Pruppacher, H. R. and Klett, J. D.: Microstructure of atmospheric clouds and precipitation, in:
609 *Microphysics of Clouds and Precipitation*, Springer, 9-55, 1978.

610 Resch, F. and Afeti, G.: Film drop distributions from bubbles bursting in seawater, *Journal of*
611 *Geophysical Research: Oceans*, 96, 10681-10688, 1991.

612 Reynolds, R. W., Smith, T. M., Liu, C., Chelton, D. B., Casey, K. S., and Schlax, M. G.: Daily high-
613 resolution-blended analyses for sea surface temperature, *Journal of climate*, 20, 5473-5496, 2007.

614 Saha, S., Moorthi, S., Wu, X., Wang, J., Nadiga, S., Tripp, P., Behringer, D., Hou, Y., Chuang, H., and
615 Iredell, M. D.: The NCEP Climate Forecast System Version 2, *Journal of Climate*, 27, 2185-2208,
616 <http://dx.doi.org/10.1175/JCLI-D-12-00823.1>, 2014.

617 Seethala, C., Zuidema, P., Edson, J., Brunke, M., Chen, G., Li, X. Y., Painemal, D., Robinson, C.,
618 Shingler, T., and Shook, M.: On assessing ERA5 and MERRA2 representations of cold - air outbreaks
619 across the Gulf Stream, *Geophysical research letters*, 48, e2021GL094364, 2021.

620 Shi, R., Xu, F., Liu, L., Fan, Z., Yu, H., Li, H., Li, X., and Zhang, Y.: The effects of ocean surface waves
621 on global intraseasonal prediction: case studies with a coupled CFSv2. 0–WW3 system, *Geoscientific*
622 *Model Development*, 15, 2345-2363, 2022.

623 Smith, R. K.: On the theory of CISK, *Quarterly Journal of the Royal Meteorological Society*, 123, 407-
624 418, 1997.

625 Song, Y., Qiao, F., Liu, J., Shu, Q., Bao, Y., Wei, M., and Song, Z.: Effects of sea spray on large-scale
626 climatic features over the Southern Ocean, *Journal of Climate*, 1-51, 2022.

627 Spiel, D. E.: More on the births of jet drops from bubbles bursting on seawater surfaces, *Journal of*
628 *Geophysical Research: Oceans*, 102, 5815-5821, 1997.

629 Thorpe, S.: Bubble clouds and the dynamics of the upper ocean, *Quarterly Journal of the Royal*
630 *Meteorological Society*, 118, 1-22, 1992.

631 Troitskaya, Y., Kandaurov, A., Ermakova, O., Kozlov, D., Sergeev, D., and Zilitinkevich, S.: The “bag
632 breakup” spume droplet generation mechanism at high winds. Part I: Spray generation function, *Journal*
633 *of physical oceanography*, 48, 2167-2188, 2018.

634 Van Eijk, A., Kusmierczyk - Michulec, J., Francius, M., Tedeschi, G., Piazzola, J., Merritt, D., and
635 Fontana, J.: Sea - spray aerosol particles generated in the surf zone, *Journal of Geophysical Research:*
636 *Atmospheres*, 116, 2011.

637 Veron, F.: Ocean spray, *Annu. Rev. Fluid Mech*, 47, 507-538, 2015.

638 Wallace, J. M., Mitchell, T., and Deser, C.: The influence of sea-surface temperature on surface wind in
639 the eastern equatorial Pacific: Seasonal and interannual variability, *Journal of Climate*, 2, 1492-1499,
640 1989.

641 Wang, C., Zhang, L., Lee, S.-K., Wu, L., and Mechoso, C. R.: A global perspective on CMIP5 climate
642 model biases, *Nature Climate Change*, 4, 201-205, 2014.

643 Wu, J.: Evaporation due to spray, *Journal of Geophysical Research*, 79, 4107-4109, 1974.

644 Wu, L., Cheng, X., Zeng, Q., Jin, J., Huang, J., and Feng, Y.: On the upward flux of sea - spray spume
645 droplets in high - wind conditions, *Journal of Geophysical Research: Atmospheres*, 122, 5976-5987,
646 2017.

647 Xu, X., Voermans, J., Ma, H., Guan, C., and Babanin, A. V.: A Wind-Wave-Dependent Sea Spray
648 Volume Flux Model Based on Field Experiments, *Journal of Marine Science and Engineering*, 9, 1168,
649 2021a.

650 Xu, X., Voermans, J., Liu, Q., Moon, I.-J., Guan, C., and Babanin, A.: Impacts of the Wave-Dependent

651 Sea Spray Parameterizations on Air–Sea–Wave Coupled Modeling under an Idealized Tropical Cyclone,
652 Journal of Marine Science and Engineering, 9, 1390, 2021b.

653 Yu, L., Jin, X., and Weller, R. A.: 2008: Multidecade global flux datasets from the Objectively Analyzed
654 Air-Sea Fluxes (OAFlux) Project: Latent and sensible heat fluxes, ocean evaporation, and related surface
655 meteorological variables. Woods Hole Oceanographic Institution OAFlux Project Tec, Rep,

656 Zhao, B., Qiao, F., Cavaleri, L., Wang, G., Bertotti, L., and Liu, L.: Sensitivity of typhoon modeling to
657 surface waves and rainfall, Journal of Geophysical Research: Oceans, 122, 1702-1723, 2017.

658

659

Table 1. The runtime of CFSv2.0-WW3 global experiments for 7-day forecast with different parameterizations.

7-day Forecast	Runtime (h)
SPRAY-A92	126.94
SPRAY-A15	7.60
SPRAY-GQ	7.67

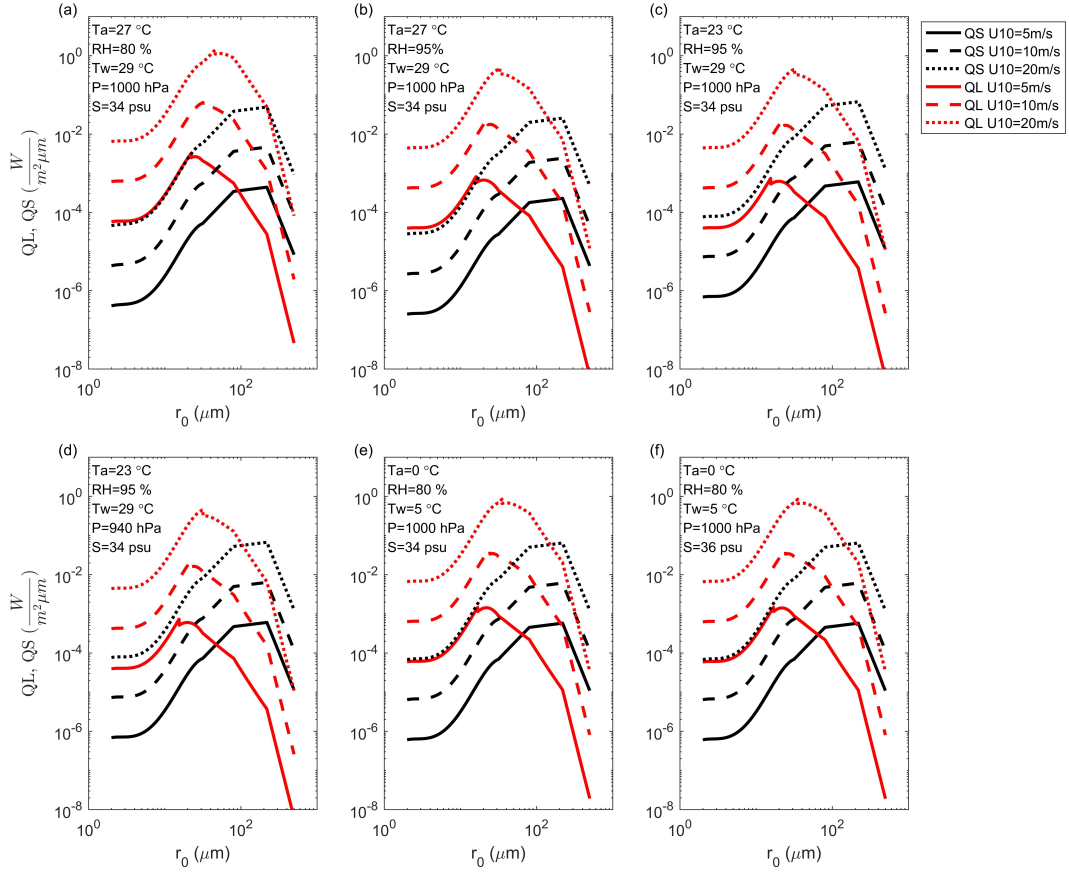


Figure 1. The radius-specific sea spray-mediated sensible (Q_S ; black) and latent (Q_L ; red) heat fluxes as functions of initial radius r_0 : U_{10} , T_a , RH , T_w , P and S are 10-m wind speed, 2-m air temperature, 2-m relative humidity, sea surface temperature, surface air pressure and surface salinity, respectively.

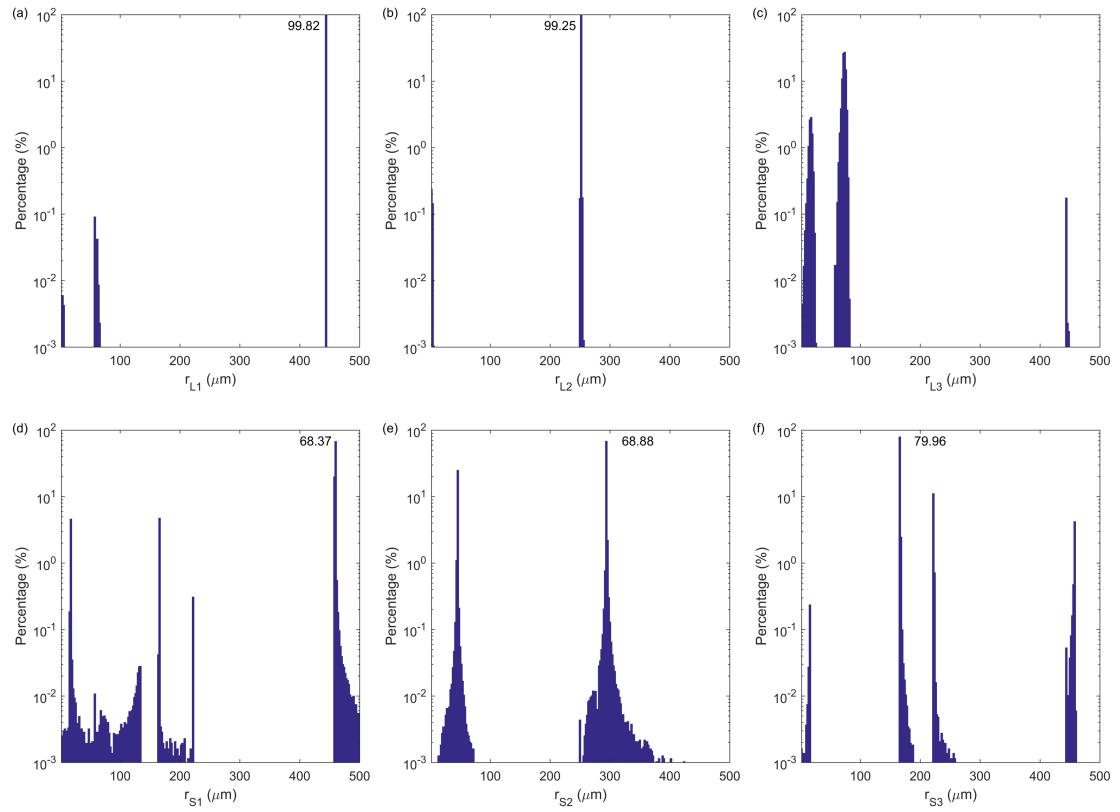


Figure 2. The distribution of occurrence frequency in percentage for GQ radius nodes: (a) the first node of latent heat flux; (b) the second node of latent heat flux; (c) the third node of latent heat flux; (d) the first node of sensible heat flux; (e) the second node of sensible heat flux; (f) the third node of sensible heat flux. The peak frequencies are marked.

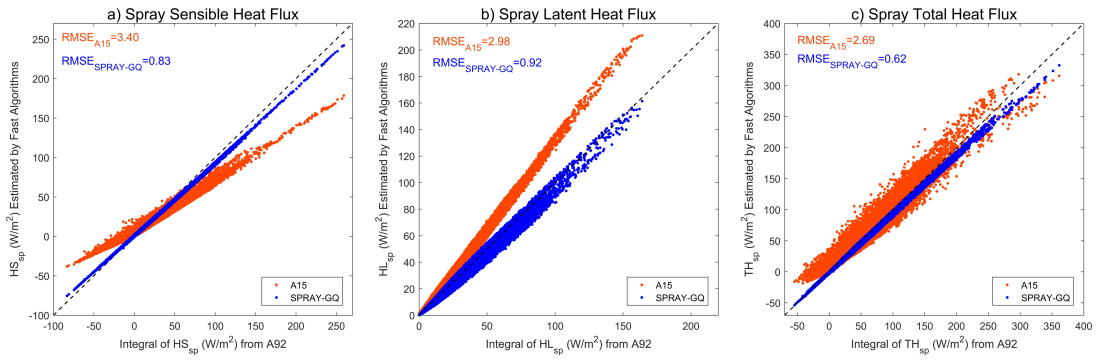


Figure 3. Scatter plots of $H_{S,SP}$ (a), $H_{L,SP}$ (b) and total heat flux $TH_{SP} = H_{S,SP} + H_{L,SP}$ (c) estimated by fast algorithms (y-axis) vs those estimated by spectral integral in microphysical parameterization (x-axis): The dotted black line is $y=x$. The corresponding RMSEs are marked in the upper left corner.

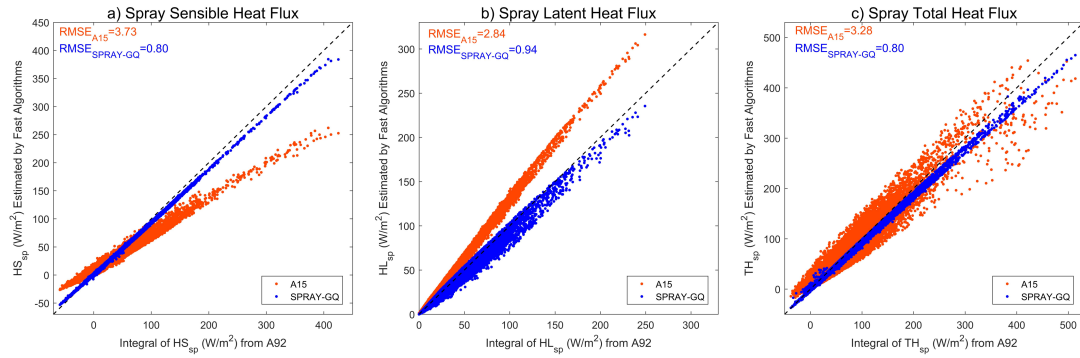


Figure 4. The same as Figure 3, but WSP10, 2-m air temperature and 2-m specific humidity of OAF flux are used.

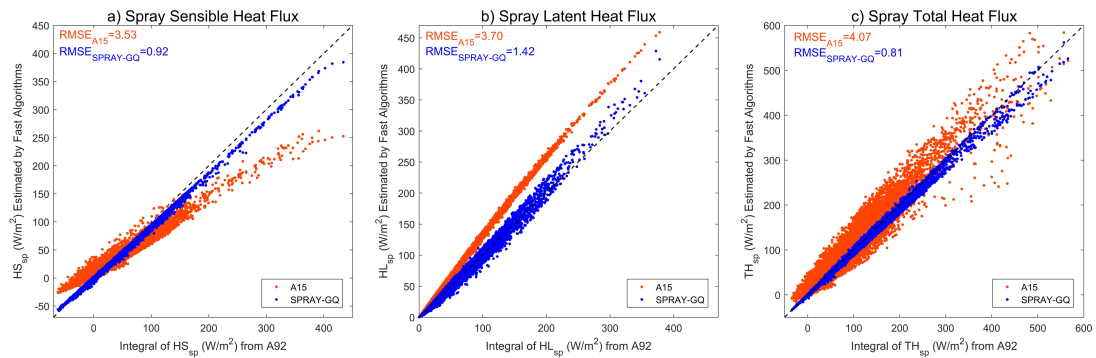


Figure 5. The same as Figure 4, but SWH is derived by WSP10 instead of ERA5 SWH.

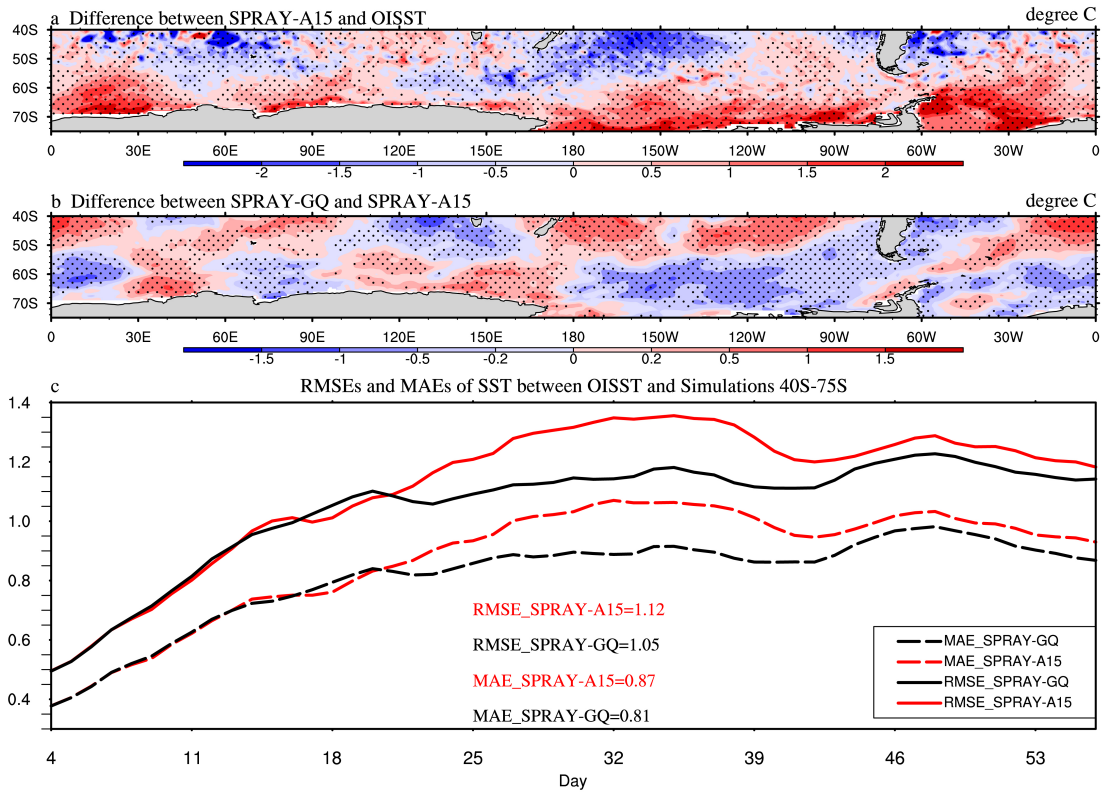


Figure 6. The 53-day average SST ($^{\circ}\text{C}$) differences between SPRAY-A15 and OISST (a; SPRAY-A15 minus OISST), the differences between SPRAY-GQ and SPRAY-A15 (b; SPRAY-GQ minus SPRAY-A15), and the time series of domain-averaged RMSE and MAE (c; 0-360 $^{\circ}\text{E}$, 40-75 $^{\circ}\text{S}$) in Jan-Feb, 2017. The first 3-day simulation is discarded. The dotted areas are statistically significant at 95% confidence level.

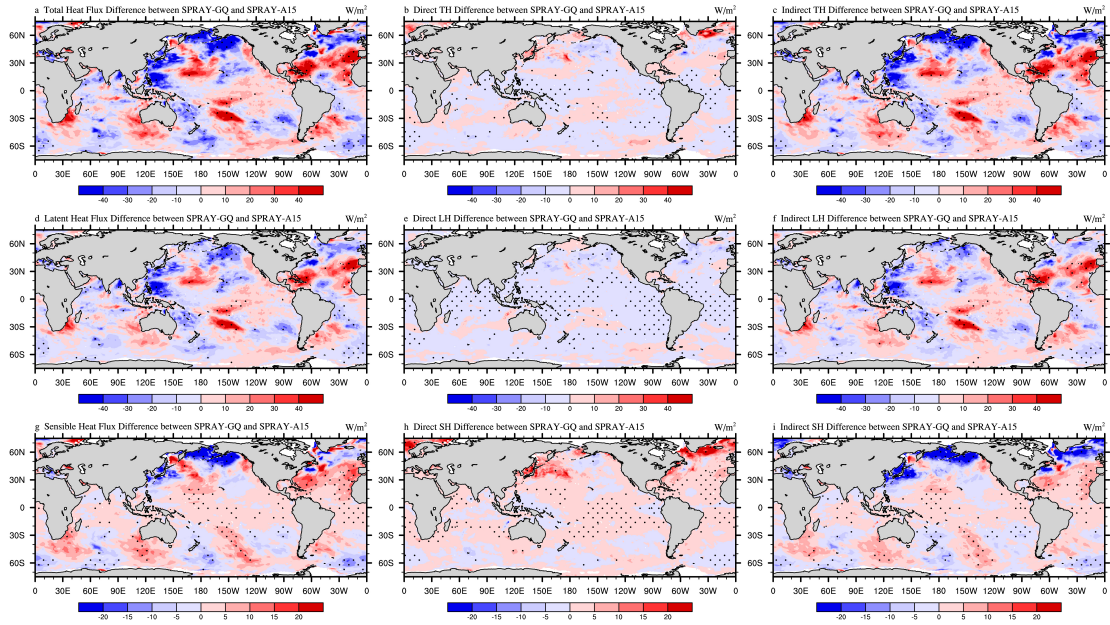


Figure 7. The 53-day average differences of total heat flux (a-c), latent heat flux (d-f), and sensible heat flux (g-i) between SPRAY-GQ and SPRAY-A15 (SPRAY-GQ minus SPRAY-A15) in Jan-Feb, 2017. The direct differences indicate sea spray-mediated heat flux differences (b, e, h), and the indirect differences indicate interfacial (bulk) heat flux differences resulted by sea spray (c, f, i). The dotted areas are statistically significant at 95% confidence level. A positive value of flux indicates an upward direction.

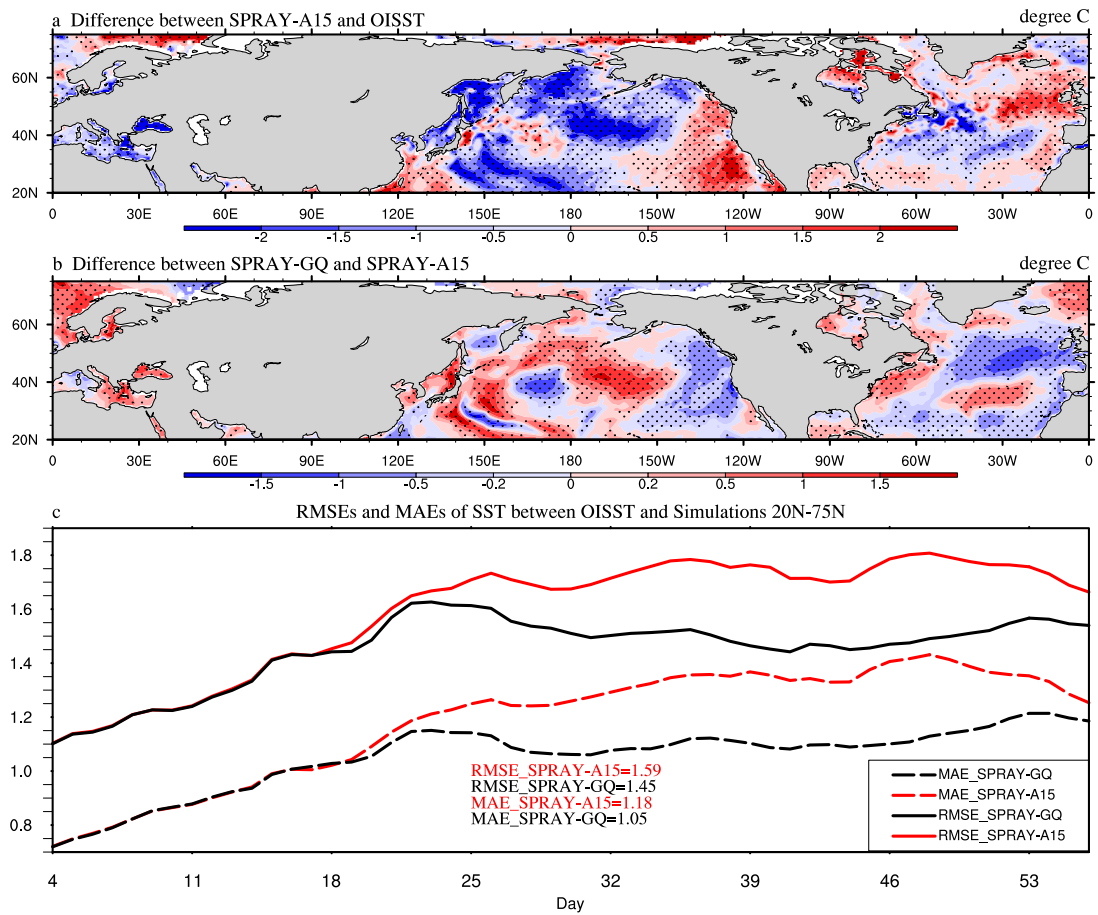


Figure 8. The same as Figure 6, but for Aug-Sep, 2018 in 0-360°E, 20-75°N.

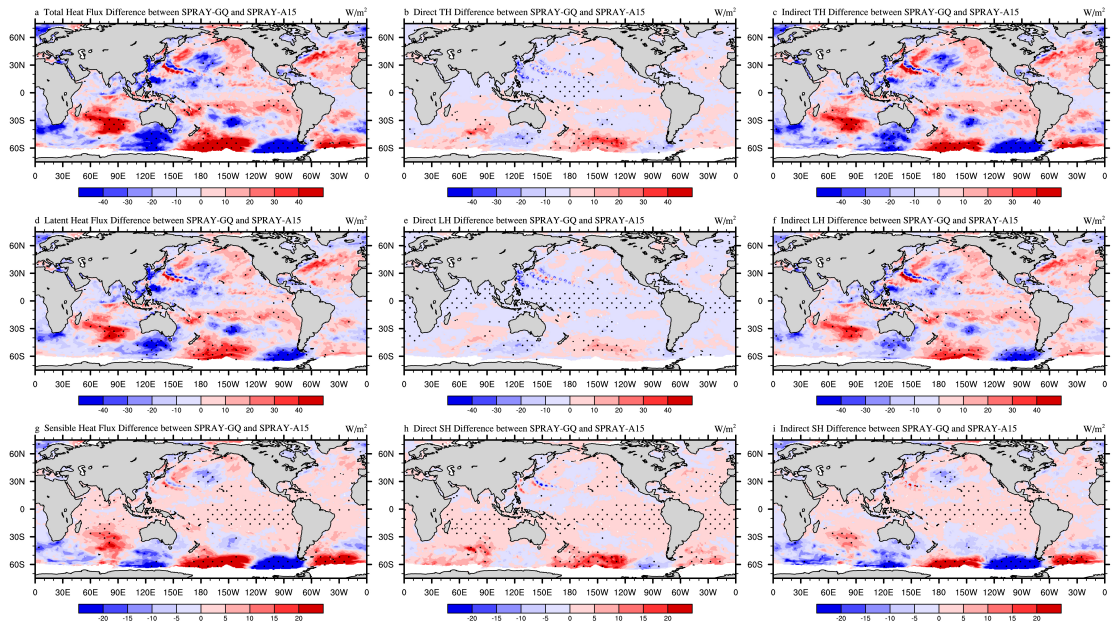


Figure 9. The same as Figure 7, but for Aug-Sep, 2018.

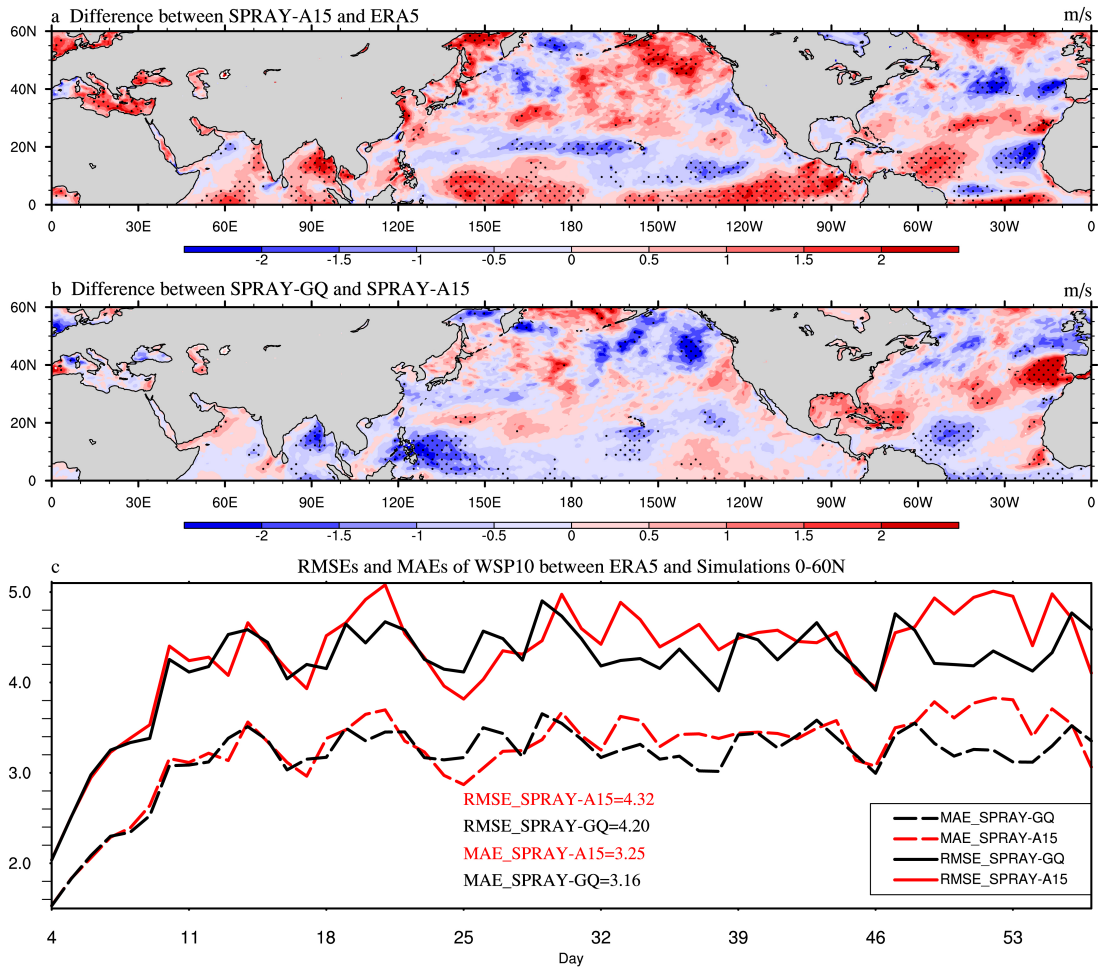


Figure 10. The 53-day average WSP10 (m/s) differences between SPRAY-A15 and ERA5 (a; SPRAY-A15 minus ERA5), the differences between SPRAY-GQ and SPRAY-A15 (b; SPRAY-GQ minus SPRAY-A15), and the time series of domain-averaged RMSE and MAE (c; 0-360°E, 0-60°N) in Jan-Feb, 2017. The first 3-day simulation is discarded. The dotted areas are statistically significant at 95% confidence level.

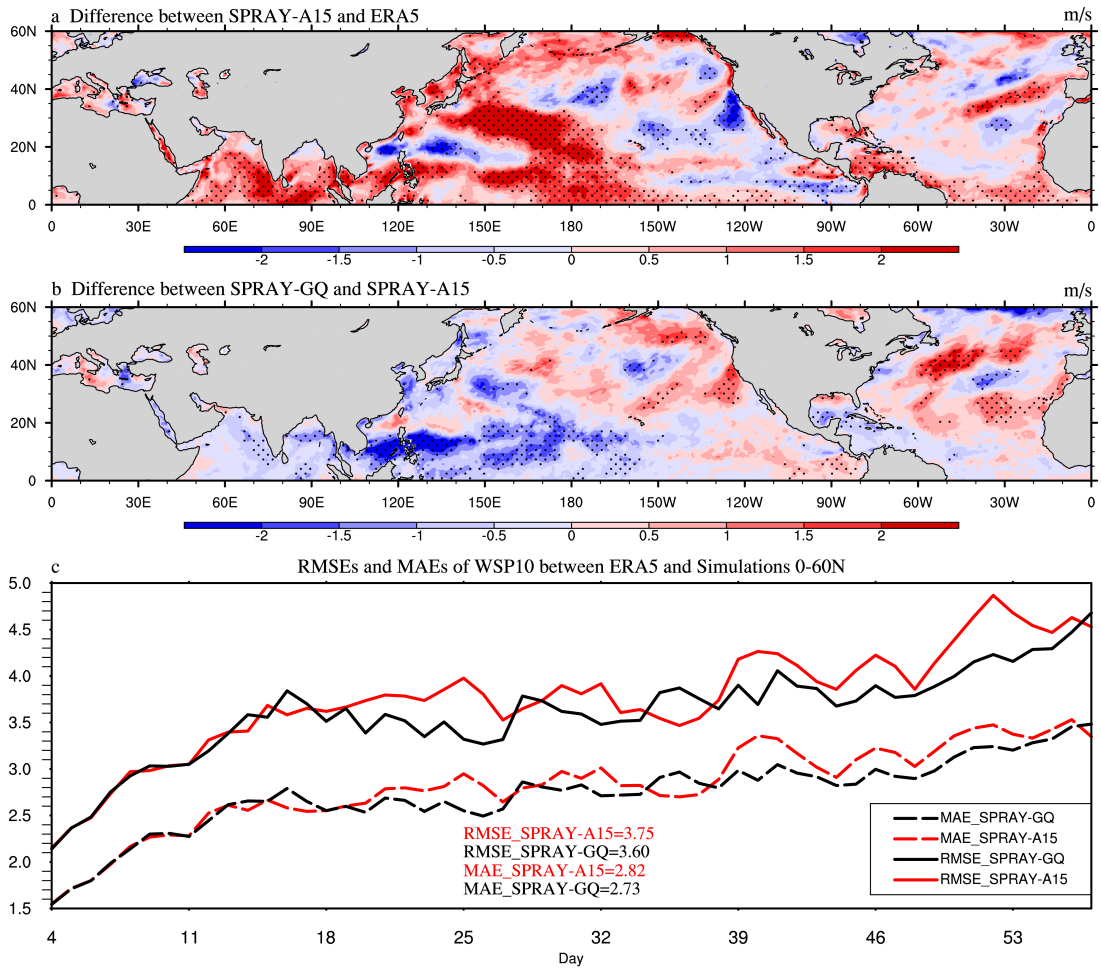


Figure 11. The same as Figure 10, but for Aug-Sep, 2018.

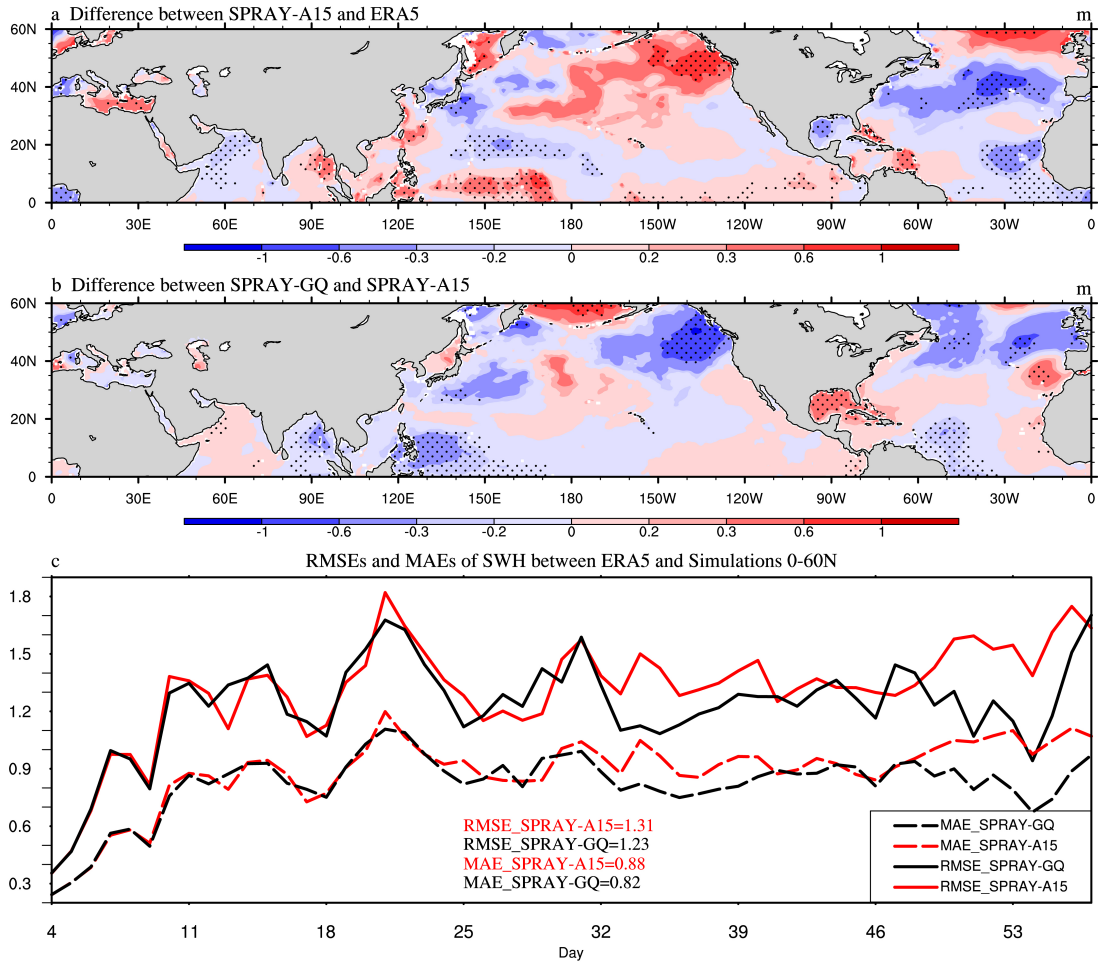


Figure 12. The 53-day average SWH (m) differences between SPRAY-A15 and ERA5 (a; SPRAY-A15 minus ERA5), the differences between SPRAY-GQ and SPRAY-A15 (b; SPRAY-GQ minus SPRAY-A15), and the time series of domain-averaged RMSE and MAE (c; 0-360°E, 0-60°N) in Jan-Feb, 2017. The first 3-day simulation is discarded. The dotted areas are statistically significant at 95% confidence level.

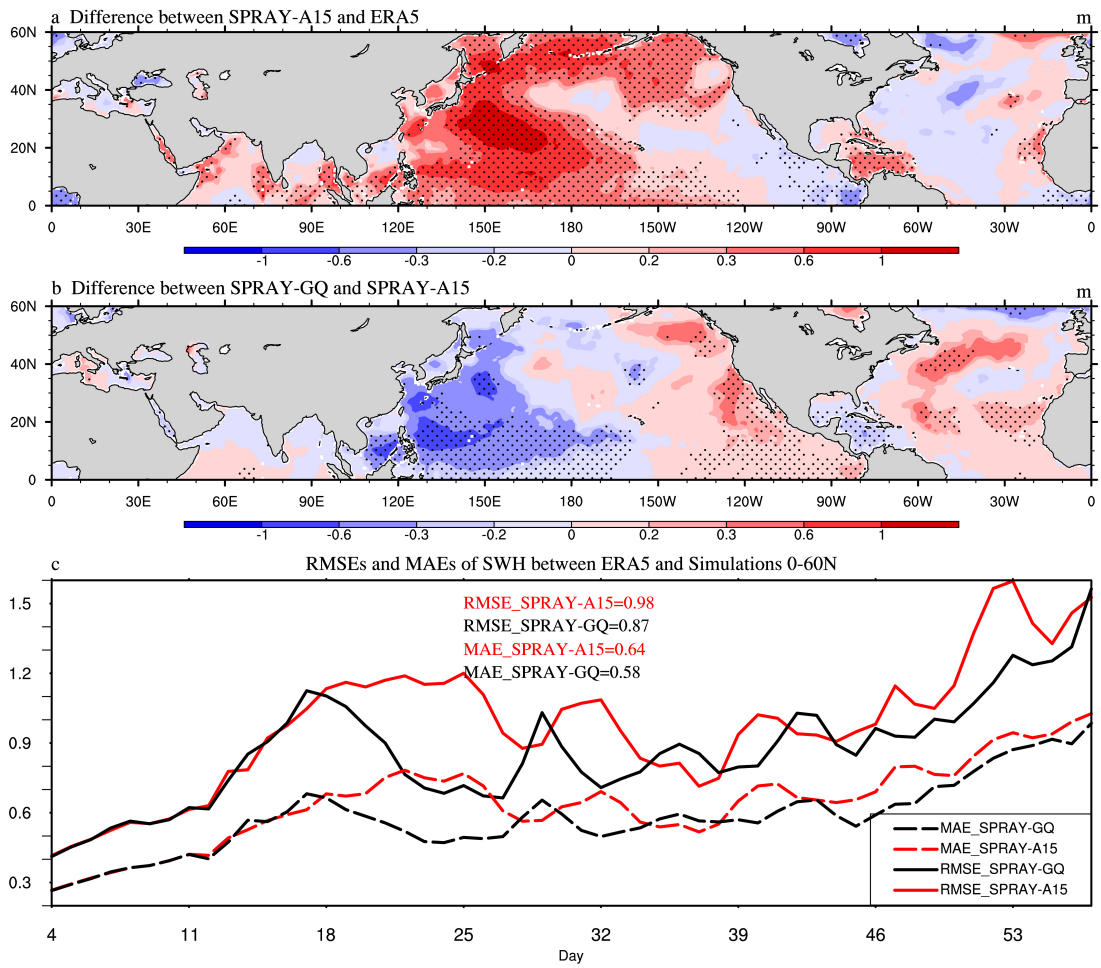


Figure 13. The same as Figure 12, but for Aug-Sep, 2018.